Cell

A Core Complex of BBS Proteins Cooperates with the GTPase Rab8 to Promote Ciliary Membrane Biogenesis

Maxence V. Nachury,[1,*] Alexander V. Loktev,[1] Qihong Zhang,[2] Christopher J. Westlake,[1] Johan Peränen,[3] Andreas Merdes,[4] Diane C. Slusarski,[5] Richard H. Scheller,[1] J. Fernando Bazan,[1] Val C. Sheffield,[2] and Peter K. Jackson[1]

[1] Genentech, Inc., South San Francisco, CA 94080, USA
[2] Department of Pediatrics and Howard Hughes Medical Institute, University of Iowa, Iowa City, IA 52242, USA
[3] Institute of Biotechnology, FIN-00014 University of Helsinki, Finland
[4] Institut de Sciences et Technologies du Médicament de Toulouse, CNRS/Pierre Fabre, 31400 Toulouse, France
[5] Department of Biological Sciences, University of Iowa, Iowa City, IA 52242, USA
*Correspondence: nachury@gene.com
DOI 10.1016/j.cell.2007.03.053

SUMMARY

Primary cilium dysfunction underlies the pathogenesis of Bardet-Biedl syndrome (BBS), a genetic disorder whose symptoms include obesity, retinal degeneration, and nephropathy. However, despite the identification of 12 BBS genes, the molecular basis of BBS remains elusive. Here we identify a complex composed of seven highly conserved BBS proteins. This complex, the BBSome, localizes to nonmembranous centriolar satellites in the cytoplasm but also to the membrane of the cilium. Interestingly, the BBSome is required for ciliogenesis but is dispensable for centriolar satellite function. This ciliogenic function is mediated in part by the Rab8 GDP/GTP exchange factor, which localizes to the basal body and contacts the BBSome. Strikingly, $Rab8^{GTP}$ enters the primary cilium and promotes extension of the ciliary membrane. Conversely, preventing $Rab8^{GTP}$ production blocks ciliation in cells and yields characteristic BBS phenotypes in zebrafish. Our data reveal that BBS may be caused by defects in vesicular transport to the cilium.

INTRODUCTION

The primary cilium is a specialized organelle found at the surface of almost every vertebrate cell. The cilium consists of an extension of the mother centriole, called the axoneme, enclosed in a membrane sheath. Recently, the cilium has become the focus of intensive studies for its role in the transduction of extracellular signals and in a constellation of genetic diseases (reviewed in Marshall and Nonaka, 2006; Scholey and Anderson, 2006; Singla and Reiter, 2006). Notably, in vertebrate cells, the Sonic Hedgehog morphogen requires the intraflagellar transport (IFT) machinery for the transport and processing of its intermediate signaling components at the tip of the primary cilium (Haycraft et al., 2005; May et al., 2005). This IFT machinery consists of two stable complexes (IFT-A and IFT-B) that have been proposed to bridge ciliary-targeted proteins to the motors responsible for bidirectional transport along the microtubule axoneme (Cole et al., 1998; Pazour et al., 1999).

A broader role of the cilium in cellular homeostasis is suggested by studies on Bardet-Biedl syndrome (BBS), a pleiotropic genetic disease whose etiology has been linked to the primary cilium (Blacque and Leroux, 2006). BBS patients are typically affected by obesity, retinal degeneration, kidney malformations, olfactory deficits, and polydactyly. While the underlying pathology of these symptoms remains enigmatic for the most part, animal models of BBS have suggested that basal body and/or cilium dysfunction is the root cause of this pleiotropic disorder. In BBS knockout mice, spermatozoa lack flagella, olfactory neurons have no cilia, and rhodopsin transport through the connecting cilium of photoreceptors frequently fails (Nishimura et al., 2004). These tissue-specific cellular defects suggest that a broad range of cilium-dependent signaling pathways may operate in various tissues through presently unknown cilium-localized receptors.

Currently, our knowledge of the molecular function of BBS proteins remains fragmentary. Twelve BBS genes have been identified without providing consistent functional clues through sequence similarities. Protein-protein interaction motifs are found in *BBS1*/*BBS2*/*BBS7* (β-propeller repeats) and *BBS4*/*BBS8* (TPR repeats). *BBS3* encodes the ARF-like GTPase ARL6, *BBS11* is identical to the E3 ubiquitin-ligase *TRIM32*, and *BBS6*/*BBS10*/*BBS12* have extensive similarity to the ATP-dependent chaperonin CCT. Clearly, the multitude of predicted functions makes a comprehensive molecular model of BBS a great challenge at present.

Nevertheless, two models have been proposed to explain the role of BBS proteins in ciliary function. The first model places BBS4 function in the cytoplasmic transport of centriolar satellites, which are nonmembranous cytoplasmic granules responsible for bringing centrin, pericentrin, Nek2, and ninein to the centrosome (Kubo et al., 1999; Dammermann and Merdes, 2002; Hames et al., 2005). It was found that BBS4 interacts with PCM-1, the core component of centriolar satellites, and with $p150^{Glued}$, a subunit of the minus-end-directed microtubule motor dynein/dynactin (Kim et al., 2004). In this model, BBS4 acts as a bridging factor between PCM-1 and dynein to bring proteins to the centrosome, and ciliary dysfunction is an indirect consequence of centrosome/basal body abnormalities.

The second model posits that BBS7 and BBS8 promote cohesion between the two IFT subcomplexes inside the primary cilium. Indeed, while IFT-A and IFT-B are transported at the same velocity from the base to the tip of nematode cilia, IFT-A and IFT-B move at distinct rates in *bbs7* or *bbs8* mutant worms (Ou et al., 2005). Although no physical interaction between IFT and BBS proteins has been reported, several BBS proteins have been found to move inside cilia at the same rates as the IFT particles (Blacque et al., 2004). In this model, ciliary dysfunction is directly linked to the role of BBS proteins inside the cilium.

In the present study, we show that the vast majority of evolutionarily conserved BBS proteins are present in a stable complex that transiently associates with PCM-1. We find that this complex functions primarily at the ciliary membrane and downstream of PCM-1. This ciliogenic function of the BBS complex is linked to the Rab8 nucleotide exchange factor, which localizes to the basal body and contacts BBS1. Following GTP loading, Rab8 targets vesicles to the cilium to promote ciliary membrane elongation. These results collectively indicate that BBS proteins likely function in membrane trafficking to the primary cilium.

RESULTS

BBS4 Localizes to the Primary Cilium of Vertebrate Cells

To gain insight into the molecular function of BBS proteins, we applied the localization and tandem affinity purification (LAP) technology to BBS4. The LAP tag consists of GFP followed by a cleavage site for the TEV protease and an S-tag (Cheeseman and Desai, 2005). First, we generated a stable clonal cell line in telomerase-immortalized RPE cells with levels of LAP-BBS4 protein expression close to those of endogenous BBS4 (Figure 1A). Consistent with a previously published report (Kim et al., 2004), LAP-BBS4 was found to fully colocalize with PCM-1 at centriolar satellites in nonciliated cells (Figures 1B and 1D). Remarkably, intense LAP-BBS4 staining was also observed inside the primary cilium of serum-starved cells, and this was accompanied by a substantial reduction in centriolar satellite staining of BBS4 (Figures 1C and 1E and see Figure S6A in the Supplemental Data available with this article online).

In addition, we observed movements of LAP-BBS4 inside the cilium at rates approaching known IFT rates in mammalian cells (Movie S1 and Figure S1) (Follit et al., 2006). This staining pattern is consistent with published reports of BBS protein localization in worms (Fan et al., 2004; Li et al., 2004) and in the connecting cilium of photoreceptor cells (Ansley et al., 2003). Although current immunological reagents against BBS proteins have failed to detect BBS proteins inside the primary cilium of vertebrate cell lines (Ansley et al., 2003; Kim et al., 2004, 2005; M.V.N. and A.V.L., unpublished data), this is likely to reflect technical difficulties in the fixation and processing of intraciliary antigens (see Follit et al., 2006, for a precedent). It should be noted that while PCM-1 colocalizes with BBS4 at centriolar satellites in the cytoplasm, no PCM-1 signal is found inside the primary cilium under any fixation conditions (Figure 1C and data not shown). BBS4 is therefore distributed between two pools inside the cell: one at centriolar satellites (with PCM-1) and the other inside the cilium (without PCM-1).

Seven of the Most Conserved BBS Proteins Form a Stable Complex that Binds PCM-1 and Tubulin

Next we purified the endogenous BBS4-associated proteins by tandem affinity purification. Surprisingly, in addition to BBS4, we recovered stoichiometric amounts of BBS1, BBS2, BBS5, BBS7, BBS8, and BBS9, as well as substoichiometric amounts of PCM-1 and α/β-tubulin (Figure 1F). Protein identification was performed by mass spectrometry, and peptide coverage was greater than 30% for each protein, supporting the high significance of all the hits (Table S1).

To determine the supramolecular organization of these nine proteins, we subjected them to a number of hydrodynamic analyses. First, the eluate of LAP-BBS4 from the anti-GFP beads was loaded on a sucrose gradient and separated by velocity sedimentation. Remarkably, all seven BBS proteins were found to fractionate together in stoichiometric proportions with a sedimentation coefficient of 14 S (Figure 2A). Meanwhile, α/β-tubulin peaked at its known value of 5 S, and PCM-1 spread across many fractions centering around 11 S. Gel filtration chromatography of the same material also showed cofractionation of the seven BBS proteins and separation from PCM-1 (Figure S2A). These data demonstrate the existence of a stable heptameric complex consisting of BBS1, BBS2, BBS4, BBS5, BBS7, BBS8, and BBS9, which we name the BBSome. The apparent molecular weight of the BBSome (438 kDa) calculated from its measured Stokes radius (78 Å) and sedimentation coefficient (14 S) is in close agreement with its predicted molecular weight of 470 kDa (Figure S2B).

In addition, gel filtration of testis extract shows that all BBSome subunits we tested cofractionate, and no free pool of those subunits was detected (Figure 2B). Again, PCM-1 was clearly separated from the BBSome, and the non-BBSome protein BBS3 eluted at the exclusion volume. The absence of a free pool of BBSome subunits

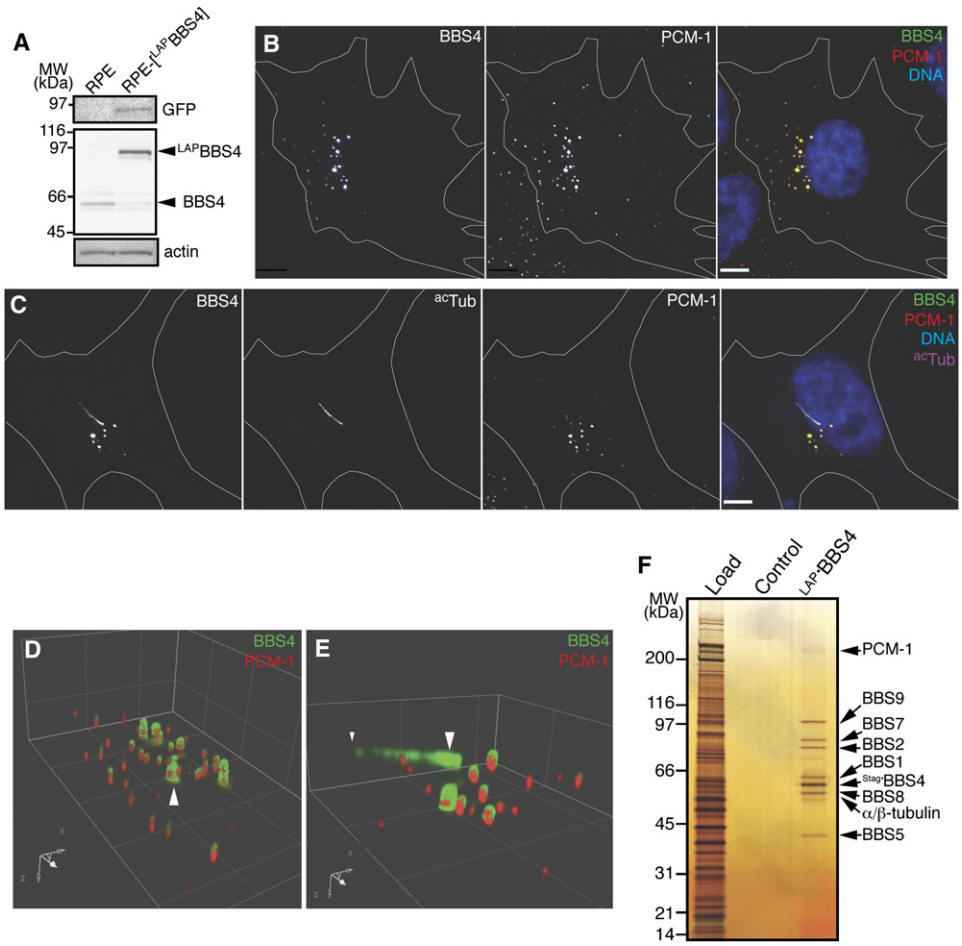

Figure 1. BBS4 Localizes to the Primary Cilium and Associates with BBS1, -2, -5, -7, -8, -9, PCM-1, and α/β-Tubulin

(A) RPE or RPE-[^{LAP}BBS4] cell extracts were immunoblotted for GFP, BBS4, and actin. The ^{LAP}BBS4 protein in RPE-[^{LAP}BBS4] cells is present at 1.8-fold over endogenous BBS4 in RPE cells, while the endogenous BBS4 protein in RPE-[^{LAP}BBS4] cells is downregulated by a factor of three compared to RPE cells.

(B and C) RPE-[^{LAP}BBS4] cells were immunostained for GFP, PCM-1, and acetylated α-tubulin. Nuclei were stained with Hoechst 33258, and cell contours were outlined in the micrographs. The cell in (B) has not grown a primary cilium, and BBS4 staining fully overlaps with PCM-1, whereas in the ciliated cell shown in (C), BBS4 also localizes to the primary cilium (overlap of green and violet seen as white signal). Scale bars, 5 μm.

(D and E) Magnified 3D surface views of centriolar satellites and cilium. Perspective is from the lower left corner of panels (B) and (C), respectively. The mother centriole/basal body is marked by a large arrowhead, and the tip of the cilium is marked by a small arrowhead. Grid unit is 5 μm.

(F) ^{LAP}BBS4-containing complexes were purified on α-GFP antibody beads followed by cleavage with TEV protease and recovery on S-protein agarose. Eluates were resolved on 4%–12% NuPAGE gels and silver stained.

strongly suggests that these seven proteins act as a single functional entity in testes.

To gain insight into the architecture of the BBSome, we tested most of the 42 possible binary interactions between BBSome subunits by cotransfection/coimmunoprecipitation experiments (Figure S3). We found two near-quantitative interactions (BBS2/BBS7 and BBS9/BBS8) as well as several moderate interactions (BBS9/BBS4, BBS9/BBS1, BBS9/BBS2, and BBS9/BBS5). Thus, BBS9 may be the central organizing subunit of the BBSome (Figure S3C).

Finally, we note that these seven subunits are among the eight most conserved BBS proteins across ciliated organisms (Table S2 and Inglis et al., 2006), whereas PCM-1 is limited to deuterostomia and absent in invertebrates and protozoa. The remarkable conservation of the BBSome and the biochemical separation of the core BBSome from PCM-1 suggest that the functions of PCM-1 and the BBSome may not fully overlap.

Functional Relationship between the BBSome and Centriolar Satellites

To examine the contribution of the BBSome to centriolar satellite function, we performed siRNA-mediated depletion of each BBSome subunit as well as PCM-1 and analyzed four markers of centriolar satellite assembly or function: PCM-1 localization to centriolar satellites, BBS4

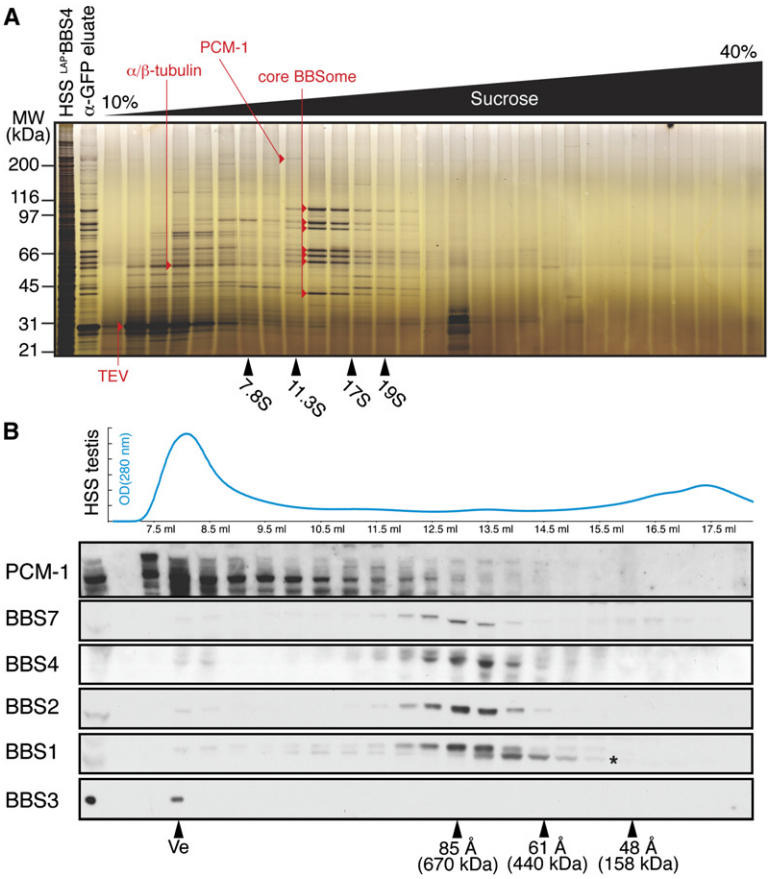

Figure 2. Seven of the Eight Most Conserved BBS Proteins Are Present in a Stable Complex

(A) The native eluate of ^{LAP}BBS4 was fractionated by sedimentation velocity on a linear 10%–40% sucrose density gradient. Fractions were resolved on 4%–12% NuPAGE gels and silver stained. Sedimentation coefficient markers were run simultaneously on an identical gradient.

(B) Testis extract was fractionated by size exclusion chromatography, and fractions were immunoblotted for PCM-1, BBS1, BBS2, BBS3, BBS4, and BBS7. A crossreacting band in the BBS1 immunoblot is indicated by an asterisk. Relative total protein concentration is shown as a graph of absorbance at 280 nm (top). The excluded volume (Ve) and the elution volumes of individual Stokes radius markers are indicated at the bottom of the panel.

recruitment to centriolar satellites, centrin targeting to the centrosome, and growth of a primary cilium (acetylated α-tubulin staining). As expected, depletion of PCM-1 (Figure 3B) led to the disappearance of centriolar satellites (Figure 3A), loss of centrin from centrosomes (Figure S4A and Dammermann and Merdes, 2002), and greatly diminished ciliation (Figure 3D and Mikule et al., 2007).

We then turned our attention to BBSome subunits. The most striking effects were seen upon depletion of BBS1 and BBS5. Three markers of PCM-1 function were left unaffected by depletion of BBS1 or BBS5 (Figure 3C and Figure S8B): PCM-1 and BBS4 still localize to centriolar satellites (Figure 3A and Figure S8A), and centrin and pericentrin are still targeted to centrosomes (Figure S4). However, ciliation is dramatically affected by the absence of BBS1 and BBS5 (Figure 3D and Figure S8C). These results unequivocally demonstrate that the BBSome promotes ciliogenesis without regulating centriolar satellite function. The effects of PCM-1 and BBS1 depletion on ciliogenesis are quite specific, as loss of BBS1 or PCM-1 did not affect cell cycle exit as judged by the drop in phospho-Rb levels (Figure S5). The most parsimonious model in agreement with the published literature predicts that the BBSome is transported by centriolar satellites to the basal body, where it separates from PCM-1 and performs its essential ciliogenic function at the basal body and/or inside the cilium.

The BBSome Associates with the Ciliary Membrane

If the BBSome separates from centriolar satellites before entering the primary cilium, one would expect its physical state to change between these two compartments. We tested this hypothesis by pre-extracting cells with a panel of detergents before fixation and processing for immunofluorescence. Extraction of cellular membranes with the nonionic detergent Triton X-100 was found to dramatically reduce the levels of BBS4 inside the cilium while leaving the levels of BBS4 at centriolar satellites unchanged (Figure 4A and Figure S6B). This behavior is reminiscent of the previously observed extractability of IFT20 (Follit et al., 2006) and suggests that the BBSome may be associated with the ciliary membrane in vivo.

The membrane association of the BBSome was then validated by subcellular fractionation experiments. First, BBS4 and PCM-1 were found to largely partition with the heavy P100 fraction (Figure 4B). To firmly establish the existence of a membrane-associated pool of the BBSome, the P100 fraction was fractionated on a sucrose flotation gradient (Figure 4C). The low-density fractions of the gradient (fractions 1 through 5) were found to contain large amounts of vesicular markers (clathrin heavy chain and coatomer subunit β-COP), whereas cytoplasmic pools of these proteins remained at the bottom of the gradient. Remarkably, over 40% of BBS4 or PCM-1 was found in the low-density

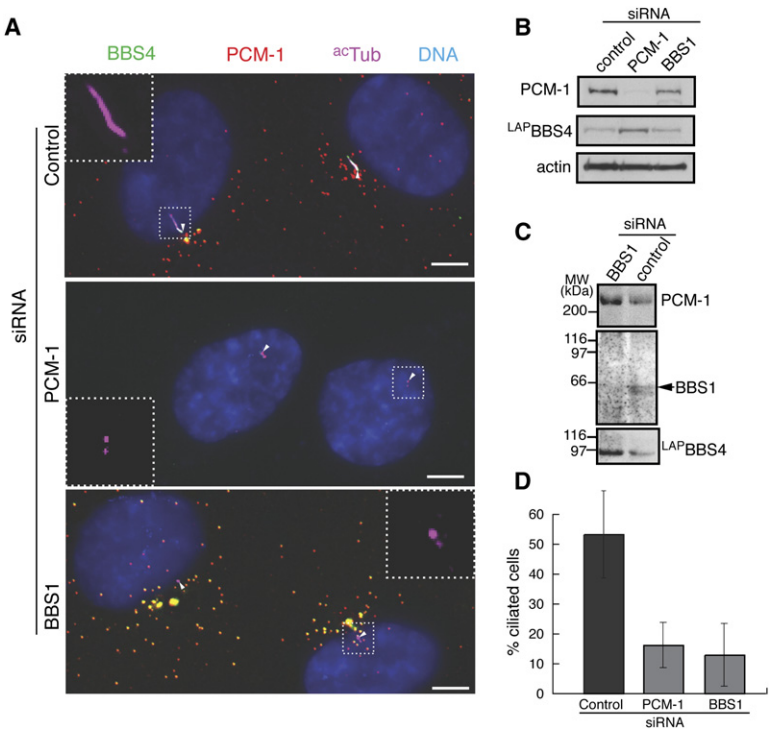

Figure 3. The Ciliogenic Function of the BBSome Lies Downstream of PCM-1

(A) RPE-[^{LAP}BBS4] cells depleted of PCM-1 or BBS1 by siRNA or control depleted cells were serum-starved to trigger ciliogenesis and immunostained for GFP (^{LAP}BBS4), PCM-1, and acetylated α-tubulin. Nuclei were stained with Hoechst 33258. Acetylated α-tubulin is present in the primary cilium (top panel) and at the centrioles (lower panels) and is shown in the insets. The mother centriole/basal body is indicated by a small white arrowhead. Cells in the top row (control) have grown primary cilia (rods in ^{ac}Tub channel), while the cells in the middle and lower rows (depleted of PCM-1 and BBS1, respectively) have failed to grow cilia (the ^{ac}Tub antibody only recognizes centrioles in these cells). Scale bar, 5 μm.

(B) Protein extracts from cells treated with siRNA directed against PCM-1, BBS1, or control siRNA were immunoblotted for PCM-1, GFP (^{LAP}BBS4), and actin (loading control). PCM-1 protein is specifically depleted by the corresponding siRNA, and BBS4 protein levels are unaffected by PCM-1 or BBS1 siRNA.

(C) α-GFP immunoprecipitates from RPE-[^{LAP}BBS4] cells treated with BBS1 siRNA or control siRNA were probed for PCM-1, GFP (^{LAP}BBS4), and BBS1 by western blotting.

(D) Depletion of PCM-1 or BBS1 prevents ciliogenesis. Cilia were counted by scoring acetylated α-tubulin-positive structures greater than 1 μm in length. 53.2% (317/579) of control siRNA-treated cells were ciliated versus 12.8% (71/493) of BBS1 siRNA-treated cells and 16.1% (85/502) of PCM-1 siRNA-treated cells. Error bars represent SD between fields.

vesicle-containing fractions of the gradient. Finally, Triton X-100 treatment of the P100 fraction reduced the proportion of floating clathrin heavy chain and BBS4 5-fold (Figure 4D).

Together these data show that the BBSome associates with membranous structures in vivo. This membrane-bound pool of the BBSome likely exists at the primary cilium but may also extend to the periciliary base (see the pool of BBS4 around the basal body in the right panel of Figure S6A).

BBS5 Contains Two Pleckstrin Homology-like (PH-like) Domains and Binds to Phosphoinositides

To better understand the function of the BBSome at the ciliary/preciliary membranes, we attempted to identify the lipid-binding subunit(s) of the BBSome. If membrane association is germane to the function of the BBSome, one would expect the lipid-binding subunit to be preferentially retained in divergent ciliated organisms that may have lost other BBSome subunits. Remarkably, the genome of the apicomplexan *Toxoplasma gondii* contains only a single BBSome subunit ortholog: *BBS5* (Table S2).

Using a combination of highly sensitive repeat-detection tools and secondary structure prediction routines applied to an evolutionarily diverse set of BBS5 orthologs (Figures S7A and S7B), we were able to extend the 50 amino-acid-long DM16 repeats (Li et al., 2004) to 125 amino-acid-long stretches (Figures 5A and 5B) whose nearest protein fold relatives are the PH-like domains PH-GRAM (Begley et al., 2003) and GLUE (Teo et al., 2006) (Figure 5C). Phosphoinositides play various roles in vesicular transport, signal transduction, and actin cytoskeleton remodeling (Di Paolo and De Camilli, 2006), and PH-GRAM/GLUE domains bind phosphoinositides at an atypical basic pocket compared to other membrane-seeking PH domains (Teo et al., 2006). Molecular modeling of the individual PH-B (PH-BBS5) repeats using superposed PH-GRAM and GLUE domain structures as templates yields compelling predictions for positively charged binding pockets in each PH-B domain (Figure S7C).

To validate our structural prediction, we directly assayed phosphoinositide specificity of the recombinant PH-B domains (BBS5$^{PH\text{-}B1}$ and BBS5$^{PH\text{-}B2}$) on PIP-blots (Dowler et al., 2002). Figure 5D shows that while GST does not produce any signal in this assay, BBS5 and BBS5$^{PH\text{-}B1}$ bound most strongly to PtdIns(3)P and phosphatidic acid. Although the relevance of this interaction was not examined in detail, we found that BBS5 is required for ciliation (Figures S8A–S8C) and inhibition of 3-phosphoinositides production by the pan-PI3 kinase inhibitor LY294002 prevented ciliation (Figures S8D–S8F). These experiments collectively suggest that BBS5 binding to phosphoinositides may be critical for ciliogenesis.

The BBSome Associates with Rabin8 at the Basal Body

To explore further links of the BBSome to membrane trafficking to the cilium, we searched our list of

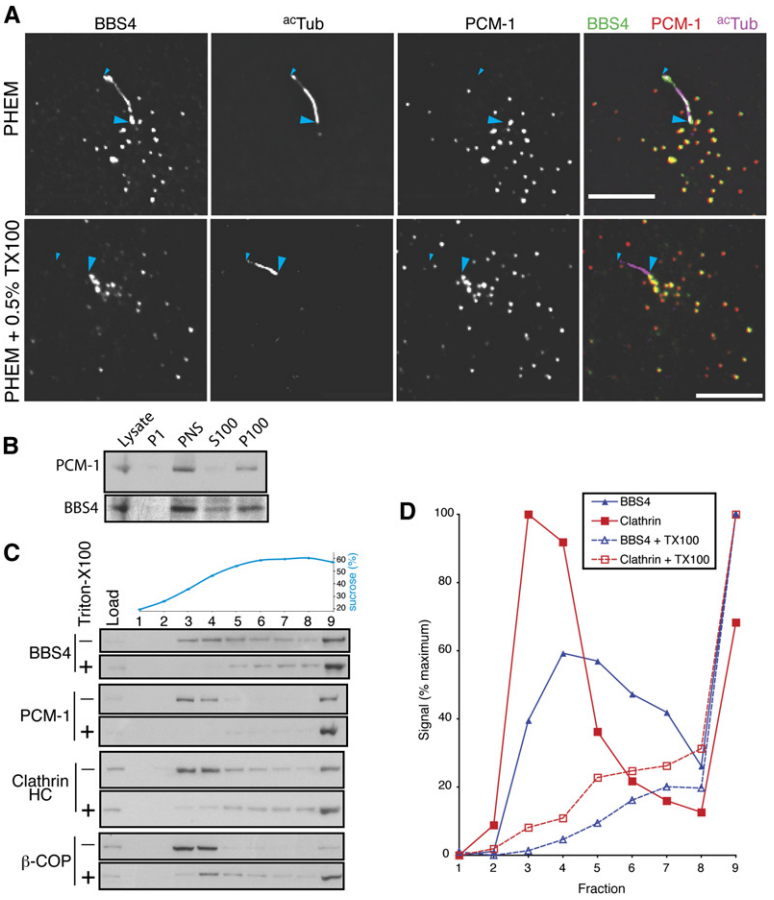

Figure 4. The BBSome Associates with the Ciliary Membrane

(A) Before fixation, RPE-[^{LAP}BBS4] cells were extracted with 0.5% Triton X-100 in PHEM (lower panel) or PHEM alone (upper panel) for 30 s. While the staining of BBS4 at centriolar satellites is unaffected by detergent treatment, the intraciliary pool of BBS4 is washed away by Triton X-100 pre-extraction. The mother centriole/basal body is marked by a large blue arrowhead, and the tip of the cilium is marked by a small blue arrowhead. Scale bar, 5 μm.

(B) Total extract (Lysate), 1000 × g pellet (P1), 1000 × g supernatant (PNS), 100,000 × g pellet (P100), and 100,000 × g supernatant (S100) were collected, and one equivalent of each fraction was immunoblotted for PCM-1 and GFP (^{LAP}BBS4).

(C) The P100 fraction from RPE-[^{LAP}BBS4] cells was separated by equilibrium flotation on a discontinuous sucrose gradient. Membrane-containing fractions are found in the low-density portion of the gradient, whereas proteic complexes stay at the bottom of the gradient. Individual fractions were immunoblotted for GFP (^{LAP}BBS4), PCM-1, clathrin heavy chain, and β-COP, and the sucrose concentration was inferred from the refractive index. Inclusion of 1% Triton X-100 in the gradient causes membrane markers as well as BBS4 and PCM-1 to repartition into the high-density fractions.

Band intensities of the GFP and clathrin blots were quantitated and plotted in the graph shown in (D).

substoichiometric factors associated with the BBSome. The most striking hit was Rabin8 (Figure S9), a guanosyl exchange factor (GEF) for Rab8 with high similarity to the yeast protein Sec2p (Hattula et al., 2002). Generally, small GTPases of the Rab family facilitate vesicular trafficking between specific compartments by promoting the docking and fusion of transport vesicles to their target compartment (Zerial and McBride, 2001). In the case of Rab8 and its yeast ortholog Sec4p, GTP loading by Rabin8/Sec2p promotes Rab8/Sec4p association with post-Golgi vesicles and targets these vesicles to polarized areas of the plasma membrane (Huber et al., 1993; Walch-Solimena et al., 1997; Ang et al., 2003).

We confirmed our LC-MS/MS analysis of the LAP-BBS4 eluate by immunoblotting Rabin8 in eluates from α-GFP immunoprecipitates of RPE-[LAP-BBS4] or RPE cells or naive IgG immunoprecipitate of RPE-[LAP-BBS4] cells (Figure 6A). We then sought to determine whether Rabin8 interacted directly with a BBSome subunit. Figure 6B and Figure S9D show that while BBS1 binds to Rabin8, none of the other BBSome subunits bound Rabin8, and BBS1 failed to interact with Rabin8 lacking the last 164 amino acids. These results show that the BBS1 subunit of the BBSome associates with the C terminus of Rabin8.

We next asked where the BBSome/Rabin8 interaction takes place inside the cell. While immunological reagents against Rabin8 failed to detect a reproducible localization, we found that stably expressed GFP-Rabin8 localizes to the edge of membrane protrusions, to vesiculo-tubular structures in the cytoplasm and to the centrosome in RPE cells (Figure 6C and Hattula et al., 2002). Since Rabin8 was not found inside the primary cilium or at centriolar satellites, it appears that the BBSome contacts Rabin8 at the centrosome/basal body, at the same time the BBSome starts to associate with membranous structures (Figure 4A and Figure S6). Finally, when Rabin8 was depleted by siRNA (Figure 6D), ciliation was reduced and BBS4 was lost from centriolar satellites (Figure 6E).

Rab8^{GTP} Enters the Cilium and Promotes Ciliary Membrane Growth

Since Rabin8 is required for ciliogenesis, the loading of GTP onto Rab8 by Rabin8 may be necessary for ciliogenesis. We tested this model by expressing several variants of Rab8 in ciliated cells (Figure 7A). Surprisingly, GFP-Rab8 localizes to the primary cilium in all ciliated cells. This localization was also observed with the hydrolysis-deficient Rab8[Q67L] variant but not with the GDP-locked Rab8[T22N] variant (Figure 7A and Figure S10). We conclude that Rab8 enters the cilium upon loading with GTP. Consistently, we found that the endogenous Rab8 localizes to the primary cilium (Figure 6F).

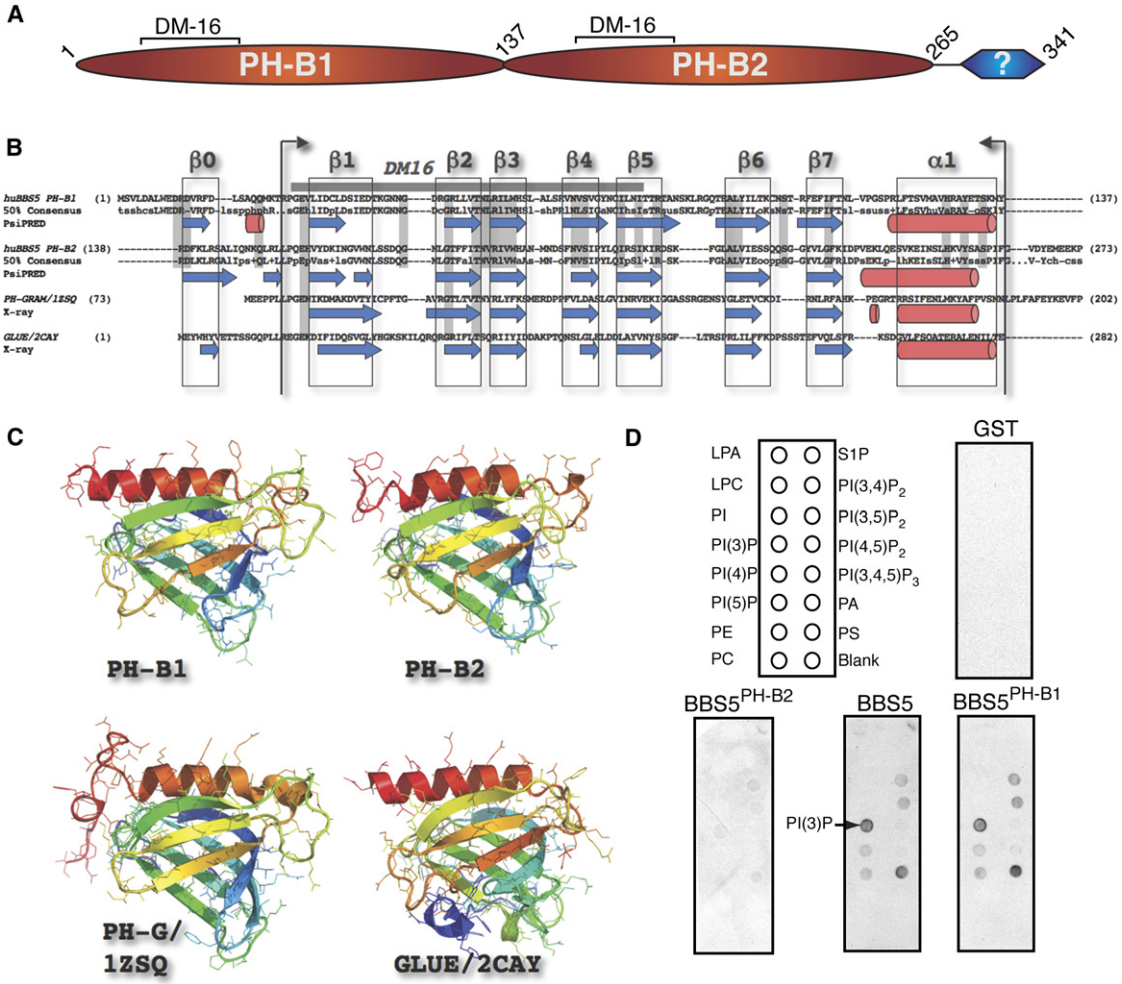

Figure 5. BBS5 Contains Novel PH-like Repeats and Binds to Specific Phosphoinositides In Vitro

(A) Schematic domain organization of BBS5.

(B) Structure-based alignment of the two PH-B repeats of BBS5 with the PH-GRAM domain of myotubularin-2 and GLUE domain of VPS36. The 50% consensus lines under the repeats are derived from the larger alignment of Figure S3A. PsiPRED secondary structure predictions for the BBS5 chain (α helices as red cylinders, β strands as blue arrows) are compared to the published structures of PH-GRAM and GLUE domains. The PH-like domain boundaries are shown as vertical dividers.

(C) The predicted folds of BBS5 repeats PH-B1 and PH-B2 are displayed alongside the two template structures of PH-GRAM and GLUE domains. The ribbons are color-ramped from N- (blue) to C- (red) terminus.

(D) The PH-B1 domain binds phosphoinositides in vitro. GST fusions of BBS5, BBS5[1–149], or BBS5[150–273] were used to probe PIP strips dotted with 100 nmoles of each individual phosphoinositide.

Furthermore, it is known that GDP-locked variants of small GTPases also function as specific inhibitors of their cognate GEFs. Thus, consistent with the effect of Rabin8 depletion, we found that expression of Rab8[T22N] prevented ciliation while an equivalent mutant in the endocytic GTPase Rab5 did not affect ciliation (Figure 7B). We note that the effect of Rab8[T22N] on cilium extension is quite specific, as expression of Rab8[T22N] in MDCK cells does not affect transport from the Golgi to the basolateral or apical membranes (Ang et al., 2003). Conversely, expression of the GTP-locked variant Rab8[Q67L] promoted significant elongation of both ciliary membrane (GFP-Rab8 signal) and axoneme (acetylated tubulin staining) compared to expression of wild-type Rab8 or Rab5[S34N] (Figure 7C). Following the Rab paradigm, these experiments indicate that $Rab8^{GTP}$ may promote the docking and fusion of exocytic vesicles to the base of the ciliary membrane. In addition, we observe a marked uncoupling between the length of the ciliary membrane and the length of the axoneme in a number of cells expressing GFP-Rab8 or GFP-Rab8[Q67L] (see data points away from the 1:1 line in Figure 7C). Extreme examples of uncoupling were seen in which a Rab8 tube emanated from a dot labeled with acetylated tubulin but no visible axoneme was detected (see data points intersecting the x axis in Figure 7C). Although no acetylated tubulin

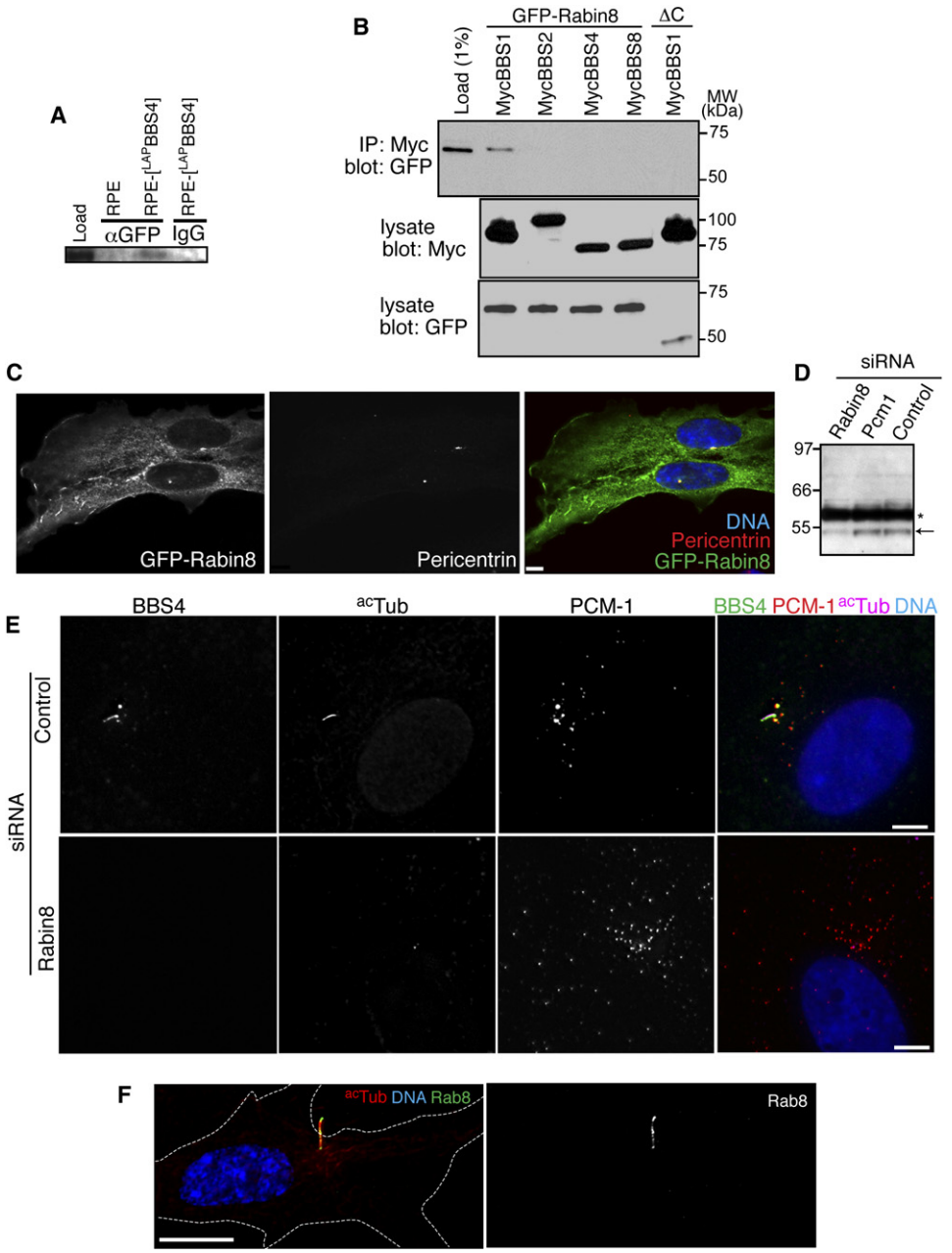

Figure 6. The BBSome Associates with Rabin8 at the Basal Body

(A) Eluates of RPE or RPE-[^{LAP}BBS4] bound to α-GFP antibody or naive IgG beads were probed for Rabin8 by western blot.

(B) Rabin8 specifically interacts with BBS1. Myc-tagged BBSome subunits were cotransfected with GFP-Rabin8 into HEK293T cells, and cell lysates were immunoprecipitated with an α-Myc antibody before western blotting with an α-GFP antibody. While Rabin8 binds to BBS1, Rabin8[1–296] (ΔC) fails to interact with BBS1 and BBS2, BBS4 and BBS8 do not bind Rabin8.

(C) GFP-Rabin8 localizes to the centrosome. A stable RPE-hTERT cell line expressing GFP-Rabin8 was established and processed for immunofluorescence staining of pericentrin. Nuclei were stained with Hoechst 33258. Scale bar, 5 μm.

(D) Protein extracts from cells treated with siRNA directed against Rabin8 or control siRNA were immunoblotted for Rabin8. The asterisk marks a 60 kDa crossreacting band.

(E) Depletion of Rabin8 prevents ciliation and disperses BBS4 staining. RPE-[^{LAP}BBS4] cells depleted of Rabin8 by siRNA were serum-starved to promote ciliation and immunostained for GFP, PCM-1, and acetylated α-tubulin. Scale bar, 2 μm. 50% (101/204) of control siRNA-treated cells were ciliated versus 23% (48/211) of Rabin8 siRNA-treated cells.

(F) Endogenous Rab8 localizes to the primary cilium. Cells were immunostained for Rab8 and acetylated α-tubulin. Nuclei were stained with Hoechst 33258. Scale bar, 5 μm.

staining was detected in these Rab8 extensions, α-tubulin is present in these extensions (Figure S11). This indicates that the rate of ciliary membrane growth promoted by Rab8GTP may overwhelm the tubulin acetylation machinery rather than axoneme elongation per se.

Finally, we tested the role of Rabin8 in the entry of Rab8 into the cilium (Figure 7D). Despite the overrepresentation of cells with intact Rabin8 in the ciliated population of Rabin8 siRNA-treated cells, we found that 42% of cilia were Rab8 negative after Rabin8 siRNA, whereas less than 3% of all cilia were Rab8-negative after control siRNA. Thus, Rabin8 is required for the entry of Rab8 into the primary cilium.

Disruption of Rab8 Function in Zebrafish Results in bbs Phenotypes

To analyze the relevance of $Rab8^{GTP}$ production to the organismic BBS phenotype, we injected mRNAs coding for Rab8 variants into one-cell zebrafish embryos. Interfering with BBS gene function in *Danio rerio* results in two very specific phenotypes: Kupffer's vesicle (KV) abnormalities and delays in the retrograde transport of melanosomes (Yen et al., 2006). Similar to the node in mammals, the KV is an embryonic ciliated structure that establishes left-right handedness (Essner et al., 2002). While expression of Rab8 and Rab8[Q67L] resulted in modest KV reduction, expression of Rab8[T22N] resulted in KV reduction similar to that brought about by *bbs2* loss of function (Figure 7E). An additional control, GDP-locked Rab10[T23N], scored just above injection background. Since Rab10 is most related to Rab8, these experiments show that inhibition of $Rab8^{GTP}$ production by Rab8[T22N] specifically affects KV formation.

Melanosomes are lysosome-related organelles that undergo actin- and microtubule-based movements between the cell periphery and the perinuclear region in response to visual cues and hormonal stimuli. We measured the time taken by melanosomes to retract from their peripheral distribution to a perinuclear accumulation upon application of epinephrine to dark-adapted embryos. Embryos injected with Rab8, Rab8[Q67L], and Rab10[T23N] behaved very similarly to uninjected embryos in this assay, whereas expression of Rab8[T22N] or inhibition of BBS2 resulted in a marked retardation of retrograde melanosome transport (Figure 7F). Given that Rab8[T22N] expression affects both melanosome retrograde transport and KV formation, we conclude that the *bbs* phenotype can be recapitulated in zebrafish by limiting the production of $Rab8^{GTP}$.

DISCUSSION

The Core BBSome: A Unifying Complex for a Genetically Heterogeneous Disease

The existence of a biochemically stable and evolutionarily conserved complex of seven BBS proteins greatly simplifies our perspective of BBS. We can now reduce the genetic complexity of BBS from 12 known genes to two highly conserved entities, the core BBSome and the small GTPase ARL6/BBS3. Meanwhile, other BBS genes are limited to chordates or vertebrates (Table S2) and are likely to be specific regulators of the BBSome and/or ARL6. Indeed, we have already found that certain chordate-specific BBS genes participate the regulation of BBSome assembly (A.V.L., Q.Z., P.K.J., V.C.S., and M.V.N., unpublished data). One tempting generalization is that BBSome integrity may be a central unifying explanation for a single pathology with extreme nonallelic heterogeneity. In particular, some BBS patients have been found to harbor three mutated alleles in two BBS genes, and there has been suggestion that the third allele could modify penetrance or severity of the clinical phenotype (reviewed in Katsanis, 2004, and see Laurier et al., 2006, for a critical evaluation). Such a scenario could now be readily explained by the biochemical instability of a multiply crippled BBSome and would parallel the ROM1/RDS heterotetramer whose genes interact to cause digenic retinitis pigmentosa (Kajiwara et al., 1994; Loewen et al., 2001).

Beyond the BBSome: Functional Clues about the Pathophysiology of BBS

The discovery of 14 BBSome-associated proteins has provided us with many functional leads. The most enlightening factor for now is Rabin8, the Rab8GEF. Downstream of Rabin8, $Rab8^{GTP}$ is likely to promote the docking and fusion of post-Golgi vesicles to the base of the cilium. This interpretation is substantiated by the remarkable finding that expression of Rab8[T22N] in frog photoreceptors results in the aberrant accumulation of rhodopsin carrier vesicles at the base of the connecting cilium (Moritz et al., 2001). Similarly, BBS2 knockout mice frequently fail to target rhodopsin to the outer segment (Nishimura et al., 2004). This phenotypic overlap between Rab8[T22N] expression and BBS loss of function is further demonstrated in zebrafish, where these alterations yield two nonoverlapping phenotypes (melanosome retrograde transport and KV formation). In summary, it appears that the BBSome may potentiate the GEF activity of Rabin8 in vivo through direct physical association and thus lead to the recruitment of $Rab8^{GTP}$ to specific post-Golgi vesicles followed by vesicle docking and fusion to the base of the cilium and finally entry of transmembrane proteins (such as rhodopsin) into the cilium. A generalization of this model to sensory cilia in the human body yields a compelling explanation for the molecular basis of BBS: each organ-specific symptom would arise through the mistargeting of specific ciliary signaling receptors involved in homeostasis of the specific organ. While still speculative in some aspects, this model offers a number of predictions that we are currently testing.

Aside from their ciliary function, it is worth noting that BBS proteins are also required for the retrograde transport of melanosomes (Yen et al., 2006). Since melanosomes are lysosome-related organelles with no apparent relationship to the cilium, the BBSome may be involved in several vesicular transport pathways.

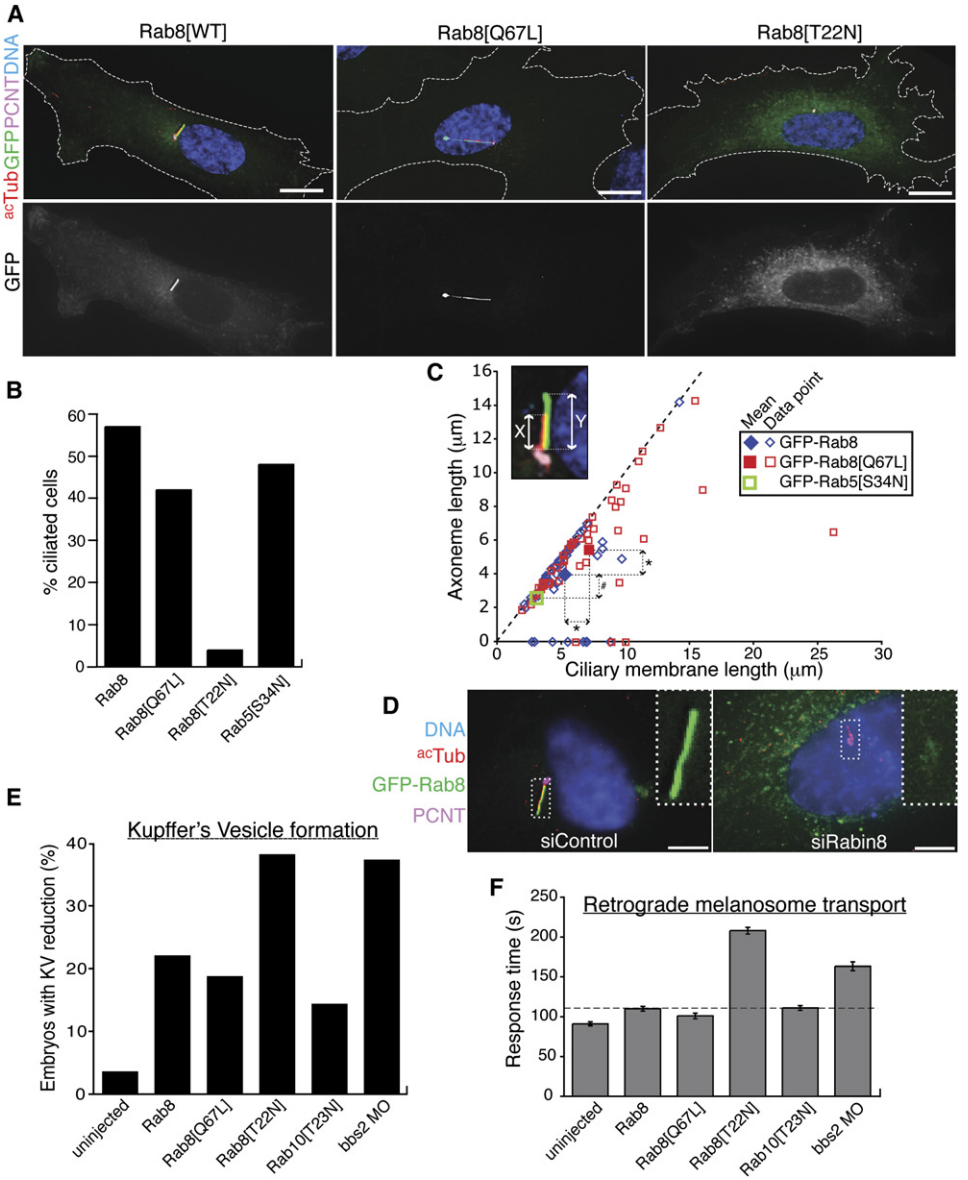

Figure 7. Rab8^{GTP} Enters the Cilium, Promotes Extension of the Ciliary Membrane, and Is Required for Ciliation

(A) Rab8 and Rab8[Q67L] localize to the primary cilium when expressed as GFP fusions in RPE cells, while Rab8[T22N]-transfected cells fail to ciliate. Forty-eight hours after transfection, cells were immunostained for GFP, PCM-1, and acetylated α-tubulin. Nuclei were stained with Hoechst 33258. Scale bar, 5 μm.

(B) Quantitation of ciliation after transfection of Rab8 variants. Over 100 cells were counted for each condition.

(C) Scatter plot of axoneme length (acetylated α-tubulin) versus ciliary membrane length (GFP-Rab8). Fifty cilia were measured for each condition. Only axoneme length was measured for the Rab5[S34N] condition. Axoneme lengths are 3.1 μm (Rab5[T34N]), 4.7 μm (Rab8), 5.8 μm (Rab8[Q67L]). The asterisk indicates a t test value $p < 0.01$, and the pound sign is for $p < 0.0001$.

(D) Rabin8 activation of Rab8 is necessary for Rab8 to enter the primary cilium. RPE cells were transfected with Rabin8 siRNA then transfected with pEGFP-Rab8 12 hr later and serum-starved after another 12 hr. Twenty-four hours after serum withdrawal, cells were immunostained for GFP, pericentrin (PCNT), and acetylated α-tubulin. Nuclei were stained with Hoechst 33258. Scale bar, 5 μm. Note that for this panel only, the contrast of the green channel in the Rabin8 siRNA subpanel was enhanced compared to the control siRNA subpanel. The inset shows the GFP-Rab8 signal inside primary cilia. 3% (2/70) of control siRNA-treated cells versus 42% (18/43) of Rabin8 siRNA-treated cells failed to target GFP-Rab8 to the cilium. A significance of $p < 10^{-6}$ was calculated on the basis of Fisher's exact test.

(E) The effect of wild-type, GTP-locked (Q67L), and a GDP-locked (T22N) Rab8 variants were tested for their effects on KV development by injecting mRNAs into one-cell embryos. 38.4% (51/133) of embryos injected with Rab8[T22N] mRNA had KV abnormalities compared to 22.2% (18/81) of Rab8- and 18.9% (7/37) of Rab8[Q67L]-injected embryos. An additional control, GDP-locked Rab10 (T23N), resulted in only 14.5% (9/62) abnormal KVs. Uninjected embryos displayed only 3.7% (4/107) KV abnormalities.

BBS5: A Possible Link between Phosphoinositides and the Cilium

The mouse mutant *tubby* is highly reminiscent of BBS mutant mice. As the name implies, these mice are obese but they also present with retinal degeneration and neurosensory hearing impairment (Ohlemiller et al., 1995). The functional overlap between tubby and BBS is even evident in *C. elegans*, where *tub-1* and *bbs-1* have been shown to act in the same genetic pathway that regulates fat deposition (Mak et al., 2006). Strikingly, Tubby proteins bind to PtdIns(3,4)P_2 and PtdIns(4,5)P_2 (Santagata et al., 2001). It is therefore tempting to speculate that phosphoinositides might regulate ciliary transport of signaling factors involved in weight control, photoreceptor function, and auditory perception.

We note that while BBS5 selectively recognizes PtdIns(3)P on PIP blots, no binding was detected in the less sensitive liposome capture assays (data not shown). However, weak protein-lipid interaction can still be physiologically relevant in the context of an entire protein complex. For example, the recently described exocytic sorting complex exomer contains a subunit capable of binding anionic lipids in PIP blots but not in liposome-binding assays (Wang et al., 2006). Still, the complete exomer clearly recognizes specific lipids when liposome-binding assays are performed in the presence of ARF^{GTP}. We are currently attempting to generate sufficient quantities of the BBSome to conduct liposome-binding experiments and determine the importance of phosphoinositides in this interaction.

The BBSome within the Cell: A Transport Cycle between Centriolar Satellites and Cilium?

The possibility of a cytoplasmic transport by centriolar satellites begs the question: why have cells evolved the complex mechanism of packaging the BBSome into proteic granules for its transport to the centrosome? One scenario is that the BBSome may have an intrinsic propensity to aggregate and/or self-associate and PCM-1 might act as a chaperone during its transport inside the cytoplasm. This property might be particularly relevant to a protein complex with ciliogenic properties: by shielding it inside the cytoplasm with PCM-1 and unmasking it at the basal body, the cell can spatially limit BBSome activation to the proximity of the basal body.

Once inside the cilium, according to studies in nematodes, the BBSome may function as an IFT cohesion factor (Ou et al., 2005). Several groups have noticed that many IFT proteins have the unusual domain combination of WD40 repeats and TPR repeats typically found in vesicular coats (Avidor-Reiss et al., 2004; Jékely and Arendt, 2006). This observation is further highlighted by the resemblance of IFT rafts to curvatureless vesicular coats at the ultrastructural level (Kozminski et al., 1993; Deane et al., 2001). Since the clathrin coat utilizes adaptors to recruit integral membrane proteins to coated pits, it is plausible that coat adaptors exist for the IFT particle. Considering that the BBSome physically interacts with phospholipids and genetically interacts with the ARF-like GTPase ARL6 (Chiang et al., 2004; Fan et al., 2004), it may well constitute such an IFT coat adaptor. Ultrastructural studies and biochemical reconstitution experiments are now in progress to address this exciting avenue.

EXPERIMENTAL PROCEDURES

Antibodies and Reagents

Antibodies were raised in rabbits against synthetic peptides from BBS2, BBS3, BBS4, and BBS7 conjugated to KLH or against recombinant GST-BBS1 and His-GFP and purified using standard protocols. All antibodies against BBS proteins were validated on testis extracts from knockout mice. Antibodies against Rab8, Rabin8, and PCM-1 were previously published (Peränen et al., 1996; Dammermann and Merdes, 2002; Hattula et al., 2002). Commercial antibodies were against β-COP (mAb M3A5), acetylated α-tubulin (mAb 6-11B-1), α-tubulin (MCAP77, Serotec), Pericentrin (ab4448, Novus), Clathrin Heavy Chain (BD #610499 for western), actin (Santa Cruz #sc-1616), V5 (mouse: Invitrogen R960-25 or rabbit: Chemicon #AB3792), GST (Molecular Probes A-5800). LY294002 was from Sigma.

Plasmids, Proteins, and Protein-Lipid Blot Overlays

BBS4 was amplified from pBs-BBS4 (cDNA clone MGC:33591) and subcloned into pEGFP-TEV-S to generate pLAP-BBS4. The LAP-BBS4 cassette was excised and subcloned into the retroviral vector pBabe-Puro (Morgenstern and Land, 1990) to generate pBabe-LAP-BBS4. Truncations of BBS5 were synthesized by DNA 2.0, Inc. in the Gateway vector pDONR221 and subcloned into pCDNA3.1-nV5 or pDEST15 (Invitrogen). GST fusions of BBS5 were expressed and purified by standard methods. PIP strips (Echelon) were probed with 1 nM of GST fusion proteins according to the manufacturer's instructions. Rab constructs were generated by Gateway subcloning into pDEST53 (Invitrogen) and a custom-made "Gatewaytized" pCS2+. Synthetic mRNA was transcribed with SP6 using the Ambion mMESSAGE mMACHINE high-yield capped RNA kit. mRNA (10 nl) (50 ng/μl) was injected into one-cell embryos.

Cell Culture, Transfections, and Quantitative RT-PCR

Stable RPE1-hTERT cell lines expressing LAP-BBS4 were generated by retroviral infection using pBabe-LAP-BBS4 according to Cheeseman and Desai (2005). siRNA duplexes against BBS1 and BBS5 were synthesized in-house following Dharmacon siGenome sequences. The most potent siRNAs were selected after assessment of mRNA knockdown by qRT-PCR. Sequences are available upon request. siRNA oligos against PCM-1 have been published (Dammermann and Merdes, 2002). RPE-[^{LAP}BBS4] cells were transfected with 100 nM siRNA duplexes using Oligofectamine (Invitrogen) following the manufacturer's instructions. Cells were shifted from 10% serum to 0.2% serum 24 hr after transfection to induce ciliation and fixed 48–72 hr posttransfection. Plasmids were transfected into RPE cells using Fugene 6 (Roche) and cells fixed 48 hr posttransfection. For qRT-PCR, Total RNA was prepared with RNeasy Mini kit (QIAGEN). RNA (100 ng) was used for qRT-PCR using QuantiTech RT-PCR kit (QIAGEN). Reactions were ran and analyzed on an ABI 7500 thermocycler.

Immunofluorescence and Microscopy

Antibodies against GFP and acetylated tubulin were directly labeled with Alexa 488 and Alexa 568, respectively. Immunofluorescence

(F) Control injected embryos (Rab8, Rab8[Q67L], and Rab10[T23N]), as well as untreated embryos, retract their melanosomes in an average time of 103.25 ± 6 s. There was minimal difference between control injected (107.3 ± 6.3 s) and uninjected (91 ± 5 s) embryos. In comparison, Rab8[T22N]-injected embryos require 208 ± 8.4 s to retract their melanosomes ($p < 0.001$). Error bars represent SD.

was performed according to standard protocols after fixation in 4% PFA. Membrane-associated proteins were pre-extracted by washing cells in PHEM buffer (60 mM PIPES, 25 mM HEPES, 10 mM EGTA, 4 mM MgSO4, pH 7.0) containing 0.5% Triton X-100 for 30 s before fixation in 4% PFA. Images were acquired on an Everest deconvolution workstation (Intelligent Imaging Innovation) equipped with a Zeiss AxioImager.Z1 and a CoolSnap CCD camera (Roper Scientific). Ten to sixteen z-sections at 0.3 μm interval were acquired, and z stacks were deconvolved and projected using Slidebook 4.1. Contrasts were adjusted identically for each series of panels.

Tandem Affinity Purification, Biochemical Fractionations, and Mass Spectrometry

Purification of the LAP-BBS4 complexes was performed according to Cheeseman and Desai (2005). To fractionate the BBSome and its interacting proteins, ^{stag}•BBS4 was cleaved off GFP after capture on anti-GFP beads by TEV cleavage and the eluate was loaded on a 12 ml 10%–40% linear sucrose gradient in LAP150 buffer (50 mM HEPES, pH 7.4, 150 mM KCl, 1 mM EGTA, 1 mM $MgCl_2$, 0.05% NP-40) and spun at 200,000 × g for 18 hr. Fractions (500 μl) were collected from the top of the gradient and concentrated by methanol/chloroform precipitation before SDS-PAGE electrophoresis. Postnuclear supernatants (PNS) were made from RPE-[^{LAP}BBS4] cells in HB (25 mM HEPES, pH 7.0, 150 mM KOAc, 2 mM MgOAc) containing 7% sucrose using a ball-bearing homogenizer (Isobiotec) with 18 μm clearance. PNS were centrifuged at 100,000 × g_{av} in a TLA100.3 rotor for 1 hr to generate the P100 and S100 fractions. The P100 was resuspended in 800 μl of HB containing 60% sucrose with the help of a dounce homogenizer fitted with a loose pestle, overlaid with 900 μl of HB with 50% sucrose and 600 μl HB with 7% sucrose, and tubes were spun in a TLS-55 rotor at 170,000 × g_{av} for 18 hr. Fractions (250 μl) were collected and processed as above. Mouse testes were homogenized by Douncing in LAP150 buffer containing 0.3% NP-40 followed by centrifugation at 100,000 × g for 1 hr. The resulting extract was fractionated on a Superose-6 10/300 GL column (GE Healthcare).

Analysis of Kupffer's Vesicle and Melanosome Transport Assay

Assays were performed according to Yen et al. (2006) following a double-blind protocol isolating the personnel performing the injection from the personnel performing the phenotype scoring.

Supplemental Data

The Supplemental Data for this article, including Supplemental Tables, Figures, and Experimental Procedures, can be found online at http://www.cell.com/cgi/content/full/129/6/1201/DC1/.

ACKNOWLEDGMENTS

We thank Jeff Salisbury for the centrin mAb, Iain Cheeseman for the LAP tag vectors and helpful discussions, Bill Lane and the Harvard Microchemistry Facility for outstanding MS analysis, and John Beck and David Hsan-jan Yen for their help with zebrafish work. We thank David Hansen, Andrew Peterson, and Suzie Scales and the Jackson lab for helpful comments on the manuscript and stimulating discussions. This work was initiated at Stanford University, where support was provided by grants from the National Institutes of Health to P.K.J. (R01-GM-54811) and a postdoctoral fellowship from the Damon Runyon Cancer Research Foundation to M.V.N. (DRG#1760-03). V.C.S. acknowledges NIH support (R01-EY-11298) and is an investigator of the Howard Hughes Medical Institute. M.V.N., A.V.L., C.J.W., R.H.S., J.F.B., and P.K.J. are employees of Genentech, inc.

Received: October 30, 2006
Revised: February 15, 2007
Accepted: March 29, 2007
Published: June 14, 2007

REFERENCES

Ang, A.L., Folsch, H., Koivisto, U.M., Pypaert, M., and Mellman, I. (2003). The Rab8 GTPase selectively regulates AP-1B-dependent basolateral transport in polarized Madin-Darby canine kidney cells. J. Cell Biol. *163*, 339–350.

Ansley, S.J., Badano, J.L., Blacque, O.E., Hill, J., Hoskins, B.E., Leitch, C.C., Kim, J.C., Ross, A.J., Eichers, E.R., Teslovich, T.M., et al. (2003). Basal body dysfunction is a likely cause of pleiotropic Bardet-Biedl syndrome. Nature *425*, 628–633.

Avidor-Reiss, T., Maer, A.M., Koundakjian, E., Polyanovsky, A., Keil, T., Subramaniam, S., and Zuker, C.S. (2004). Decoding cilia function: defining specialized genes required for compartmentalized cilia biogenesis. Cell *117*, 527–539.

Begley, M.J., Taylor, G.S., Kim, S.A., Veine, D.M., Dixon, J.E., and Stuckey, J.A. (2003). Crystal structure of a phosphoinositide phosphatase, MTMR2: insights into myotubular myopathy and Charcot-Marie-Tooth syndrome. Mol. Cell *12*, 1391–1402.

Blacque, O.E., and Leroux, M.R. (2006). Bardet-Biedl syndrome: an emerging pathomechanism of intracellular transport. Cell. Mol. Life Sci. *63*, 2145–2161.

Blacque, O.E., Reardon, M.J., Li, C., McCarthy, J., Mahjoub, M.R., Ansley, S.J., Badano, J.L., Mah, A.K., Beales, P.L., Davidson, W.S., et al. (2004). Loss of C. elegans BBS-7 and BBS-8 protein function results in cilia defects and compromised intraflagellar transport. Genes Dev. *18*, 1630–1642.

Cheeseman, I.M., and Desai, A. (2005). A combined approach for the localization and tandem affinity purification of protein complexes from metazoans. Sci. STKE *2005*, pl1. Published online January 11, 2005. 10.1126/stke.2662005pl1.

Chiang, A.P., Nishimura, D., Searby, C., Elbedour, K., Carmi, R., Ferguson, A.L., Secrist, J., Braun, T., Casavant, T., Stone, E.M., and Sheffield, V.C. (2004). Comparative genomic analysis identifies an ADP-ribosylation factor-like gene as the cause of Bardet-Biedl syndrome (BBS3). Am. J. Hum. Genet. *75*, 475–484.

Cole, D.G., Diener, D.R., Himelblau, A.L., Beech, P.L., Fuster, J.C., and Rosenbaum, J.L. (1998). Chlamydomonas kinesin-II-dependent intraflagellar transport (IFT): IFT particles contain proteins required for ciliary assembly in Caenorhabditis elegans sensory neurons. J. Cell Biol. *141*, 993–1008.

Dammermann, A., and Merdes, A. (2002). Assembly of centrosomal proteins and microtubule organization depends on PCM-1. J. Cell Biol. *159*, 255–266.

Deane, J.A., Cole, D.G., Seeley, E.S., Diener, D.R., and Rosenbaum, J.L. (2001). Localization of intraflagellar transport protein IFT52 identifies basal body transitional fibers as the docking site for IFT particles. Curr. Biol. *11*, 1586–1590.

Di Paolo, G., and De Camilli, P. (2006). Phosphoinositides in cell regulation and membrane dynamics. Nature *443*, 651–657.

Dowler, S., Kular, G., and Alessi, D.R. (2002). Protein lipid overlay assay. Sci. STKE *2002*, PL6. Published online April 23, 2002. 10.1126/stke.2002.129.pl6.

Essner, J.J., Vogan, K.J., Wagner, M.K., Tabin, C.J., Yost, H.J., and Brueckner, M. (2002). Conserved function for embryonic nodal cilia. Nature *418*, 37–38.

Fan, Y., Esmail, M.A., Ansley, S.J., Blacque, O.E., Boroevich, K., Ross, A.J., Moore, S.J., Badano, J.L., May-Simera, H., Compton, D.S., et al. (2004). Mutations in a member of the Ras superfamily of small GTP-binding proteins causes Bardet-Biedl syndrome. Nat. Genet. *36*, 989–993.

Follit, J.A., Tuft, R.A., Fogarty, K.E., and Pazour, G.J. (2006). The intraflagellar transport protein IFT20 is associated with the Golgi complex and is required for cilia assembly. Mol. Biol. Cell *17*, 3781–3792.

Hames, R.S., Crookes, R.E., Straatman, K.R., Merdes, A., Hayes, M.J., Faragher, A.J., and Fry, A.M. (2005). Dynamic recruitment of Nek2 kinase to the centrosome involves microtubules, PCM-1, and localized proteasomal degradation. Mol. Biol. Cell *16*, 1711–1724.

Hattula, K., Furuhjelm, J., Arffman, A., and Peränen, J. (2002). A Rab8-specific GDP/GTP exchange factor is involved in actin remodeling and polarized membrane transport. Mol. Biol. Cell *13*, 3268–3280.

Haycraft, C.J., Banizs, B., Aydin-Son, Y., Zhang, Q., Michaud, E.J., and Yoder, B.K. (2005). Gli2 and Gli3 localize to cilia and require the intraflagellar transport protein polaris for processing and function. PLoS Genet *1*, e53. Published online October 28, 2005. 10.1371/journal.pgen.0010053.

Huber, L.A., Pimplikar, S., Parton, R.G., Virta, H., Zerial, M., and Simons, K. (1993). Rab8, a small GTPase involved in vesicular traffic between the TGN and the basolateral plasma membrane. J. Cell Biol. *123*, 35–45.

Inglis, P.N., Boroevich, K.A., and Leroux, M.R. (2006). Piecing together a ciliome. Trends Genet. *22*, 491–500.

Jékely, G., and Arendt, D. (2006). Evolution of intraflagellar transport from coated vesicles and autogenous origin of the eukaryotic cilium. Bioessays *28*, 191–198.

Kajiwara, K., Berson, E.L., and Dryja, T.P. (1994). Digenic retinitis pigmentosa due to mutations at the unlinked peripherin/RDS and ROM1 loci. Science *264*, 1604–1608.

Katsanis, N. (2004). The oligogenic properties of Bardet-Biedl syndrome. Hum. Mol. Genet. *13*(*Spec No 1*), R65–R71.

Kim, J.C., Badano, J.L., Sibold, S., Esmail, M.A., Hill, J., Hoskins, B.E., Leitch, C.C., Venner, K., Ansley, S.J., Ross, A.J., et al. (2004). The Bardet-Biedl protein BBS4 targets cargo to the pericentriolar region and is required for microtubule anchoring and cell cycle progression. Nat. Genet. *36*, 462–470.

Kim, J.C., Ou, Y.Y., Badano, J.L., Esmail, M.A., Leitch, C.C., Fiedrich, E., Beales, P.L., Archibald, J.M., Katsanis, N., Rattner, J.B., and Leroux, M.R. (2005). MKKS/BBS6, a divergent chaperonin-like protein linked to the obesity disorder Bardet-Biedl syndrome, is a novel centrosomal component required for cytokinesis. J. Cell Sci. *118*, 1007–1020.

Kozminski, K.G., Johnson, K.A., Forscher, P., and Rosenbaum, J.L. (1993). A motility in the eukaryotic flagellum unrelated to flagellar beating. Proc. Natl. Acad. Sci. USA *90*, 5519–5523.

Kubo, A., Sasaki, H., Yuba-Kubo, A., Tsukita, S., and Shiina, N. (1999). Centriolar satellites: molecular characterization, ATP-dependent movement toward centrioles and possible involvement in ciliogenesis. J. Cell Biol. *147*, 969–980.

Laurier, V., Stoetzel, C., Muller, J., Thibault, C., Corbani, S., Jalkh, N., Salem, N., Chouery, E., Poch, O., Licaire, S., et al. (2006). Pitfalls of homozygosity mapping: an extended consanguineous Bardet-Biedl syndrome family with two mutant genes (BBS2, BBS10), three mutations, but no triallelism. Eur. J. Hum. Genet. *14*, 1195–1203.

Li, J.B., Gerdes, J.M., Haycraft, C.J., Fan, Y., Teslovich, T.M., May-Simera, H., Li, H., Blacque, O.E., Li, L., Leitch, C.C., et al. (2004). Comparative genomics identifies a flagellar and basal body proteome that includes the BBS5 human disease gene. Cell *117*, 541–552.

Loewen, C.J., Moritz, O.L., and Molday, R.S. (2001). Molecular characterization of peripherin-2 and rom-1 mutants responsible for digenic retinitis pigmentosa. J. Biol. Chem. *276*, 22388–22396.

Mak, H.Y., Nelson, L.S., Basson, M., Johnson, C.D., and Ruvkun, G. (2006). Polygenic control of Caenorhabditis elegans fat storage. Nat. Genet. *38*, 363–368.

Marshall, W.F., and Nonaka, S. (2006). Cilia: tuning in to the cell's antenna. Curr. Biol. *16*, R604–R614.

May, S.R., Ashique, A.M., Karlen, M., Wang, B., Shen, Y., Zarbalis, K., Reiter, J., Ericson, J., and Peterson, A.S. (2005). Loss of the retrograde motor for IFT disrupts localization of Smo to cilia and prevents the expression of both activator and repressor functions of Gli. Dev. Biol. *287*, 378–389.

Mikule, K., Delaval, B., Kaldis, P., Jurcyzk, A., Hergert, P., and Doxsey, S. (2007). Loss of centrosome integrity induces p38–p53–p21-dependent G1–S arrest. Nat. Cell Biol. *9*, 160–170.

Morgenstern, J.P., and Land, H. (1990). A series of mammalian expression vectors and characterisation of their expression of a reporter gene in stably and transiently transfected cells. Nucleic Acids Res. *18*, 1068.

Moritz, O.L., Tam, B.M., Hurd, L.L., Peranen, J., Deretic, D., and Papermaster, D.S. (2001). Mutant rab8 Impairs docking and fusion of rhodopsin-bearing post-Golgi membranes and causes cell death of transgenic Xenopus rods. Mol. Biol. Cell *12*, 2341–2351.

Nishimura, D.Y., Fath, M., Mullins, R.F., Searby, C., Andrews, M., Davis, R., Andorf, J.L., Mykytyn, K., Swiderski, R.E., Yang, B., et al. (2004). Bbs2-null mice have neurosensory deficits, a defect in social dominance, and retinopathy associated with mislocalization of rhodopsin. Proc. Natl. Acad. Sci. USA *101*, 16588–16593.

Ohlemiller, K.K., Hughes, R.M., Mosinger-Ogilvie, J., Speck, J.D., Grosof, D.H., and Silverman, M.S. (1995). Cochlear and retinal degeneration in the tubby mouse. Neuroreport *6*, 845–849.

Ou, G., Blacque, O.E., Snow, J.J., Leroux, M.R., and Scholey, J.M. (2005). Functional coordination of intraflagellar transport motors. Nature *436*, 583–587.

Pazour, G.J., Dickert, B.L., and Witman, G.B. (1999). The DHC1b (DHC2) isoform of cytoplasmic dynein is required for flagellar assembly. J. Cell Biol. *144*, 473–481.

Peränen, J., Auvinen, P., Virta, H., Wepf, R., and Simons, K. (1996). Rab8 promotes polarized membrane transport through reorganization of actin and microtubules in fibroblasts. J. Cell Biol. *135*, 153–167.

Santagata, S., Boggon, T.J., Baird, C.L., Gomez, C.A., Zhao, J., Shan, W.S., Myszka, D.G., and Shapiro, L. (2001). G-protein signaling through tubby proteins. Science *292*, 2041–2050.

Scholey, J.M., and Anderson, K.V. (2006). Intraflagellar transport and cilium-based signaling. Cell *125*, 439–442.

Singla, V., and Reiter, J.F. (2006). The primary cilium as the cell's antenna: signaling at a sensory organelle. Science *313*, 629–633.

Teo, H., Gill, D.J., Sun, J., Perisic, O., Veprintsev, D.B., Vallis, Y., Emr, S.D., and Williams, R.L. (2006). ESCRT-I core and ESCRT-II GLUE domain structures reveal role for GLUE in linking to ESCRT-I and membranes. Cell *125*, 99–111.

Walch-Solimena, C., Collins, R.N., and Novick, P.J. (1997). Sec2p mediates nucleotide exchange on Sec4p and is involved in polarized delivery of post-Golgi vesicles. J. Cell Biol. *137*, 1495–1509.

Wang, C.W., Hamamoto, S., Orci, L., and Schekman, R. (2006). Exomer: A coat complex for transport of select membrane proteins from the trans-Golgi network to the plasma membrane in yeast. J. Cell Biol. *174*, 973–983.

Yen, H.J., Tayeh, M.K., Mullins, R.F., Stone, E.M., Sheffield, V.C., and Slusarski, D.C. (2006). Bardet-Biedl syndrome genes are important in retrograde intracellular trafficking and Kupffer's vesicle cilia function. Hum. Mol. Genet. *15*, 667–677.

Zerial, M., and McBride, H. (2001). Rab proteins as membrane organizers. Nat. Rev. Mol. Cell Biol. *2*, 107–117.

Cell, Volume *129*

Supplemental Data

A Core Complex of BBS Proteins Cooperates with the GTPase Rab8 to Promote Ciliary Membrane Biogenesis

Maxence V. Nachury, Alexander V. Loktev, Qihong Zhang, Christopher J. Westlake, Johan Peränen, Andreas Merdes, Diane C. Slusarski, Richard H. Scheller, J. Fernando Bazan, Val C. Sheffield, and Peter K. Jackson

MW (kDa)	protein	GenBank id	peptide coverage	unique peptides
228	PCM-1	450277	31%	54
90	BBS9	74355093	37%	30
80.3	BBS7a	29029557	47%	32
79.8	BBS2	13507379	38%	23
65.1	BBS1	14042475	58%	28
62	^{Stag}BBS4	20379692	74%	37
58	BBS8	38146012	45%	20
50	β-Tubulin	12846758	34%	12
50	α-Tubulin	68402829	39%	12
39	BBS5	46988521	44%	15

Table S1: Summary of LC-MS/MS analysis of the ^{LAP}BBS4 eluate.
Proteins are listed in order of decreasing molecular weight with their GenBank id, the percentage of their amino acid sequence covered by peptides identified by MS and the number of peptides that match exclusively with this protein sequence. S-protein eluates were resolved on 4-12% gel and the gel was stained with colloidal Coomasie. Individual bands were excised and subjected to liquid chromatography coupled to tandem mass spectrometry (LC-MS/MS).

Species	Flagellum	IFT subunits	core BBSome						
			BBS1	BBS2	BBS4	BBS5	BBS7	BBS8	BBS9
mouse	YES	12	BBS1	BBS2	BBS4	BBS5	BBS7	BBS8	BBS9
zebrafish	YES	12	BBS1	BBS2	BBS4	BBS5	BBS7	BBS8	BBS9
Ciona	YES	12	BBS1	BBS2	BBS4	BBS5	BBS7	BBS8	BBS9
C.elegans	YES	12	BBS1	BBS2	BBS4	BBS5	BBS7	BBS8	BBS9
Tetrahymena	YES	12	BBS1	BBS2	BBS4	BBS5	BBS7	BBS8	BBS9
Chlamydomonas	YES	12	BBS1	BBS2	BBS4	BBS5	BBS7	BBS8	BBS9
Trypanosoma	YES	12	BBS1	BBS2	BBS4	BBS5	BBS7	BBS8	BBS9
Leishmania	YES	12	BBS1	BBS2	BBS4	BBS5	BBS7	BBS8	BBS9
Drosophila	YES	10	BBS1	-	BBS4	BBS5	-	BBS8	BBS9
Giardia	YES	11	-	-	BBS4	BBS5	-	BBS8	-
Toxoplasma	YES	8	-	-	-	BBS5	-	-	-
Plasmodium	YES*	0	-	-	-	-	-	-	-
Dictyostelium	NO	0	-	-	-	-	-	-	-
Arabidopsis	NO	0	-	-	-	-	-	-	-
rice	NO	0	-	-	-	-	-	-	-
Saccharomyces	NO	0	-	-	-	-	-	-	-

Species	Flagellum	IFT subunits	PCM-1	BBS3/ ARL6	BBS6	BBS10	BBS11/ TRIM32	CCDC28B
mouse	YES	12	PCM-1	ARL6	BBS6	BBS10	TRIM32	CCDC28B
zebrafish	YES	12	PCM-1	ARL6	BBS6	BBS10	TRIM32	CCDC28B
Ciona	YES	12	PCM-1	ARL6	BBS6	-	TRIM32	-
C.elegans	YES	12	-	ARL6	-	-	-	-
Tetrahymena	YES	12	-	ARL6	-	-	-	-
Chlamydomonas	YES	12	-	ARL6	-	-	-	-
Trypanosoma	YES	12	-	ARL6	-	-	-	-
Leishmania	YES	12	-	ARL6	-	-	-	-
Drosophila	YES	10	-	ARL6	-	-	-	CCDC28B
Giardia	YES	11	-	-	-	-	-	-
Toxoplasma	YES	8	-	-	-	-	-	-
Plasmodium	YES*	0	-	-	-	-	-	-
Dictyostelium	NO	0	-	-	-	-	-	-
Arabidopsis	NO	0	-	-	-	-	-	-
rice	NO	0	-	-	-	-	-	-
Saccharomyces	NO	0	-	-	-	-	-	-

Table S2: Conservation of BBSome subunits, associated proteins and other BBS genes or BBS modifiers in a panel of evolutionarily diverse organisms.

Orthologues were identified by reciprocal Blast using the publicly available completed genome sequences. Note that *Drosophila melanogaster*, *Giardia lamblia* and *Toxoplasma gondii* have lost certain IFT subunits and have also lost several BBSome subunits while all organisms with a full complement of IFT subunits have retained a full complement of BBSome subunits. Surprisingly, the proposed BBS modifier gene CCDC28B (Badano et al., 2006) possesses a very different pattern of evolutionary conservation from all other BBS genes.

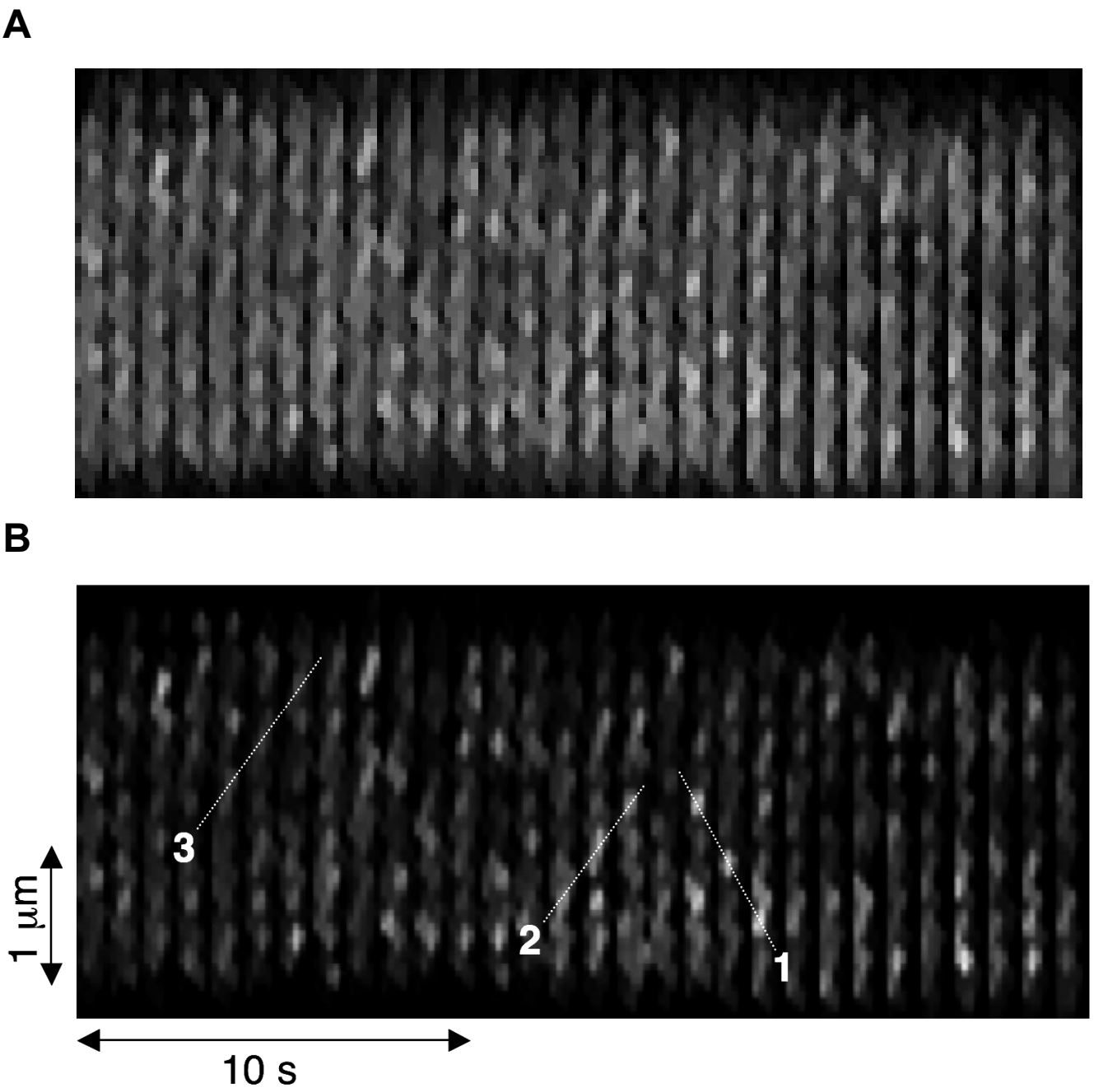

Figure S1: Motility of BBS4 inside the primary cilium.

(A) Kymograph assembled from movie S1. (B) Kymogram analysis. The rates of movement of each individual line are: R1= 0.404 μm/s (retrograde); R2= 0.303 μm/s (anterograde); R3= 0.318. μm/s (anterograde).

A

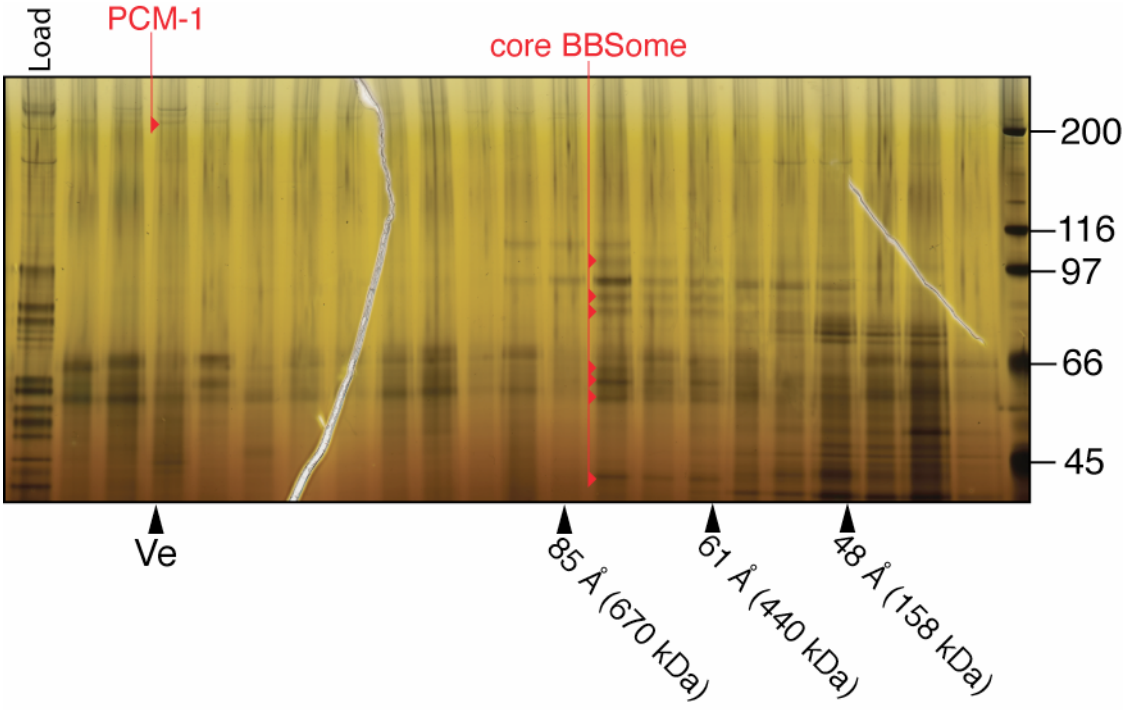

B

Measured molecular weight:	$Ma = 6\pi\eta\mathcal{N}R_sS/(1-v\rho)$ = 438 kDa
Calculated BBSome molecular weight:	ΣMW[BBS1,2,4,5,7,8,9] = 470 kDa

<u>Figure S2</u>: The calculated and apparent molecular weights of the core BBSome are in close agreement.

(A) The native eluate of ^{LAP}BBS4 was fractionated by size exclusion chromatography and fractions were resolved on 4-12 % NuPAGE gels and silver stained. The Stokes radius of the core BBSome of 78 Å was estimated from a Porath correlation generated using the elution volumes of the standards (Siegel and Monty, 1966). (B) The apparent molecular weight of the core BBSome was calculated according to (Siegel and Monty, 1966). The sum of the predicted molecular weights of the individual BBSome subunits is indicated for comparison purposes.

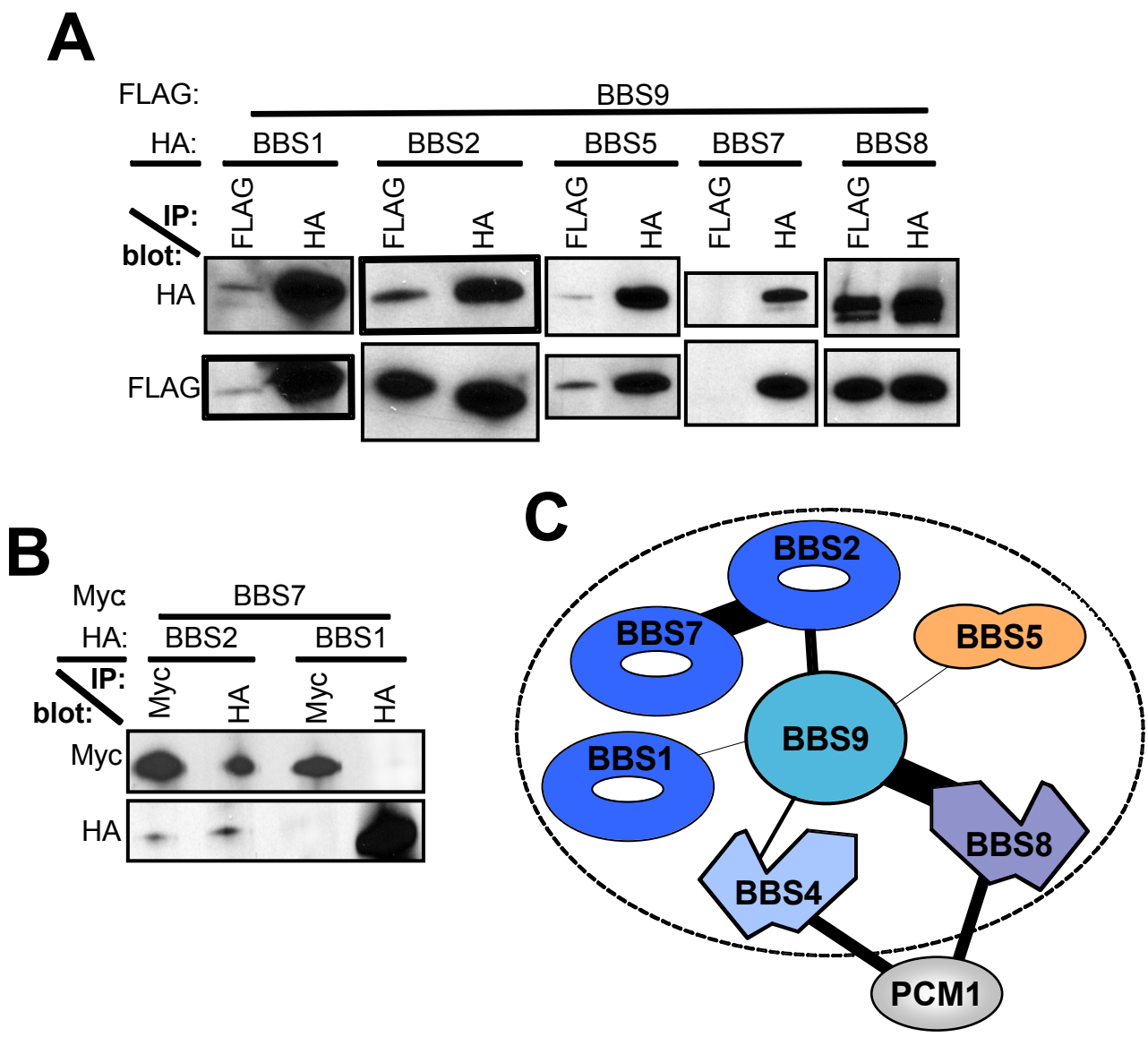

Figure S3: Interactions among BBSome subunits. Tagged BBSome subunits were cotransfected into 293T cells and reciprocal immunoprecipitations were conducted to detect protein-protein interactions. (A) BBS9 forms a stoichiometric complex with BBS8 and binds to BBS1, BBS2 and BBS5 but not BBS7. (B) BBS2 and BBS7 form a stoichiometric complex. (C) Predicted BBSome topology from protein-protein interaction mapping. The apparent strength of each interaction is depicted by the thickness of the connector. The PCM-1/BBS4 and PCM-1/BBS8 interactions were previously published (Ansley et al., 2003; Kim et al., 2004).

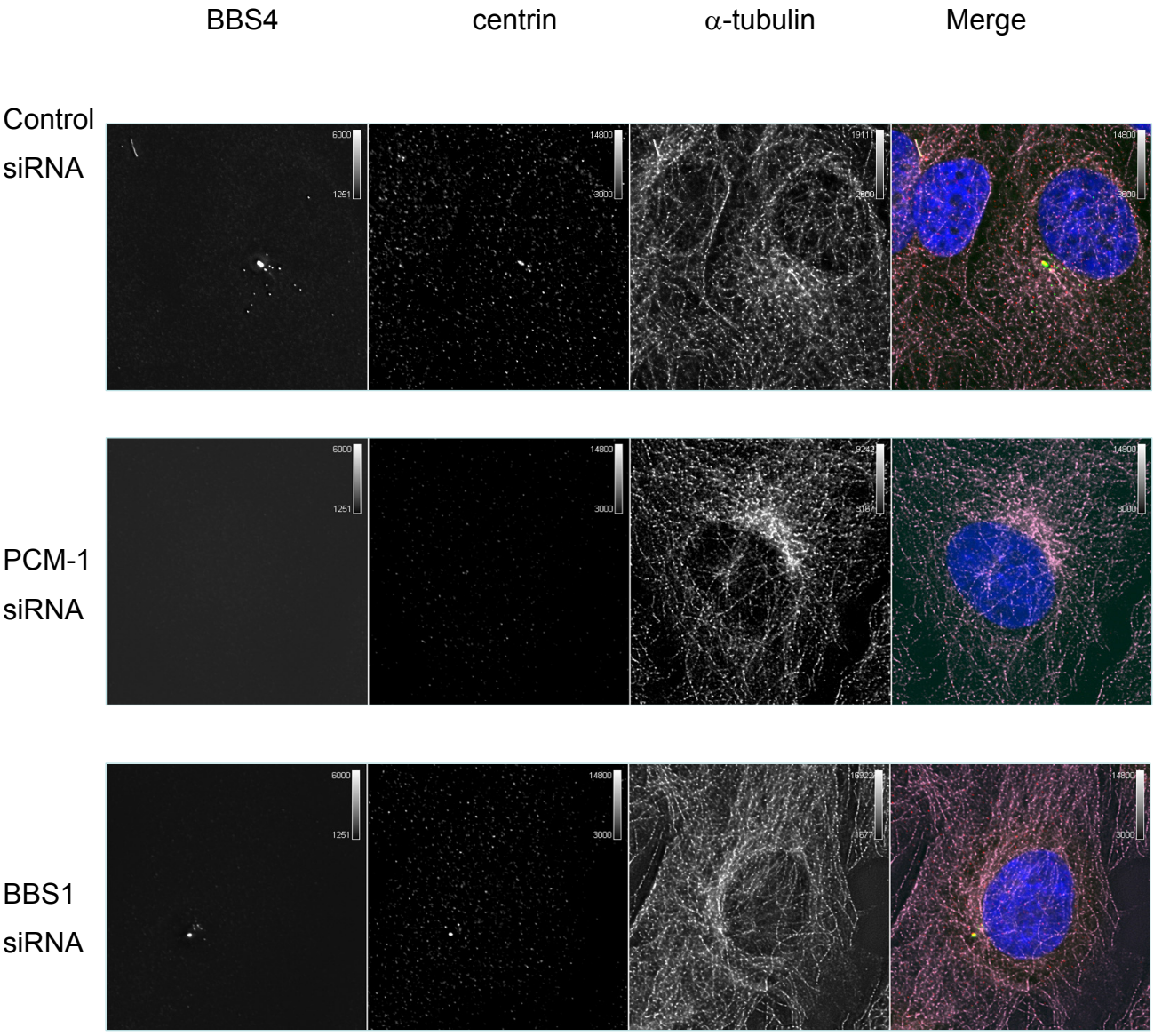

<u>Figure S4</u>: Depletion of PCM-1 specifically affects centrin targeting to the centrosome. (A) Centrin is mislocalized in cells treated with PCM-1 siRNA but not BBS1 siRNA. Cells were immunostained for GFP (green), centrin (red) and α-tubulin (pink). Nuclei were stained with Hoechst 33258 (blue).

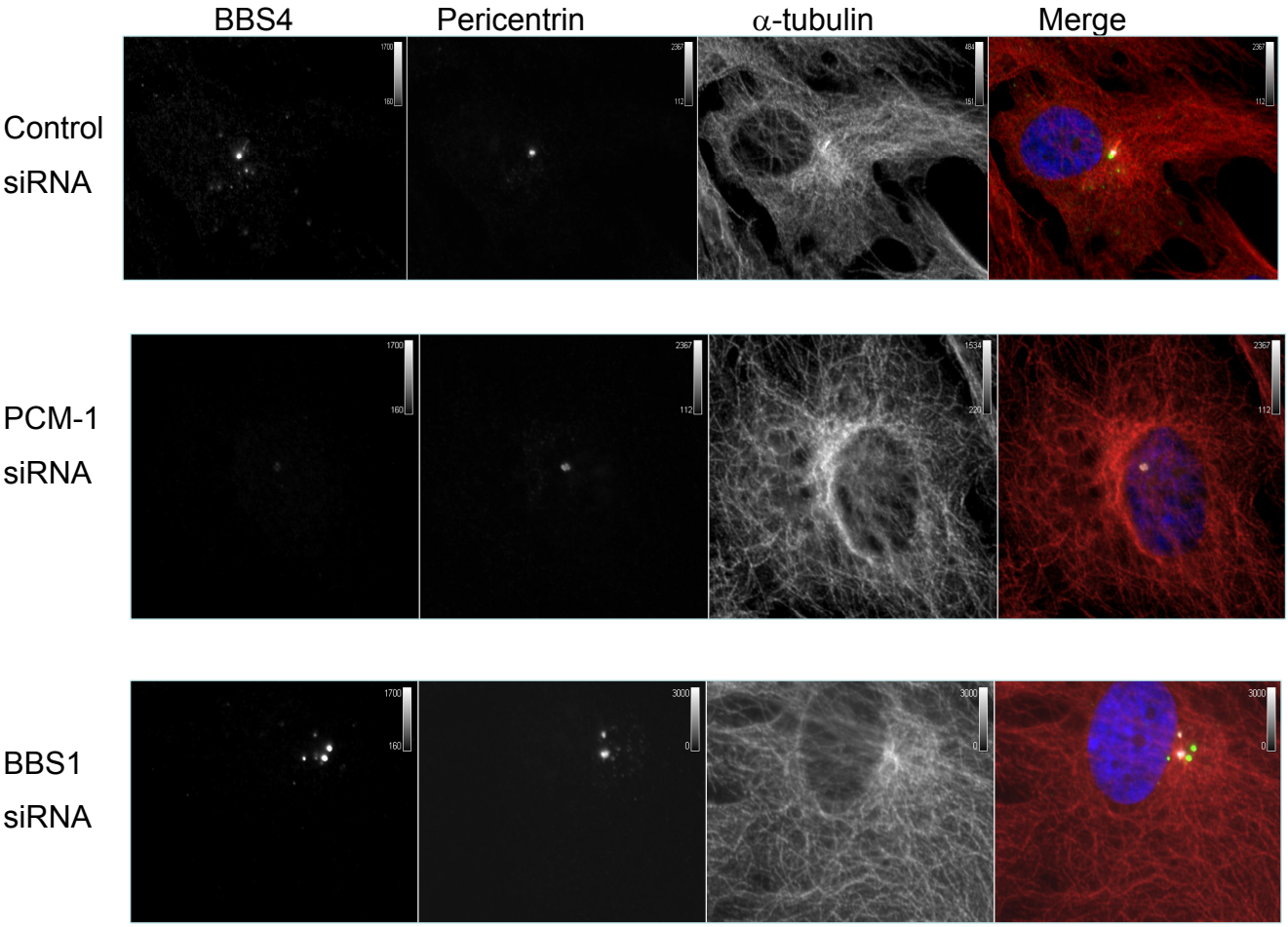

Figure S4 (followed): (B) Pericentrin levels at the centrosome are reduced in PCM-1-depleted cells but not in BBS1-depleted cells. Cells were immunostained for GFP (green), pericentrin (pink) and α-tubulin (red). Nuclei were stained with Hoechst 33258 (blue). These images were not deconvolved and represent one focal plane of capture.

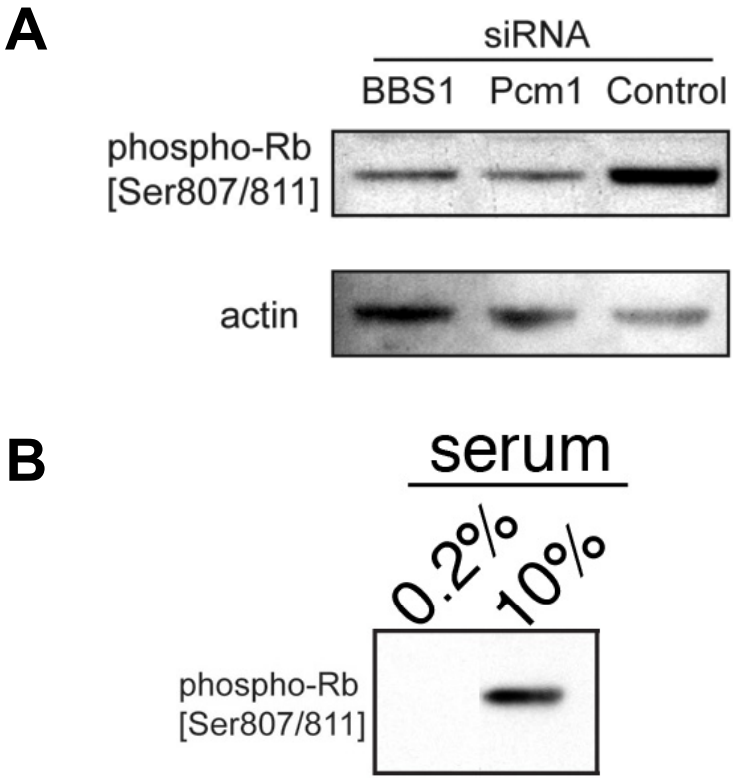

Figure S5: Depletion of BBS1 or PCM-1 does not affect cell cycle exit. (A) Protein extracts from cells visualized in Figure 3 and Figure S4 were immunoblotted for the proliferation marker phspho-Rb. Depletion of BBS1 or PCM-1 does not lead to elevated levels of phospho-Rb. (B) Extract from serum-starved cells (equivalent to control cells in panel A) and from proliferating cells were immunoblotted for phospho-Rb. Phospho-Rb is undetectable in quiescent cells at this exposure.

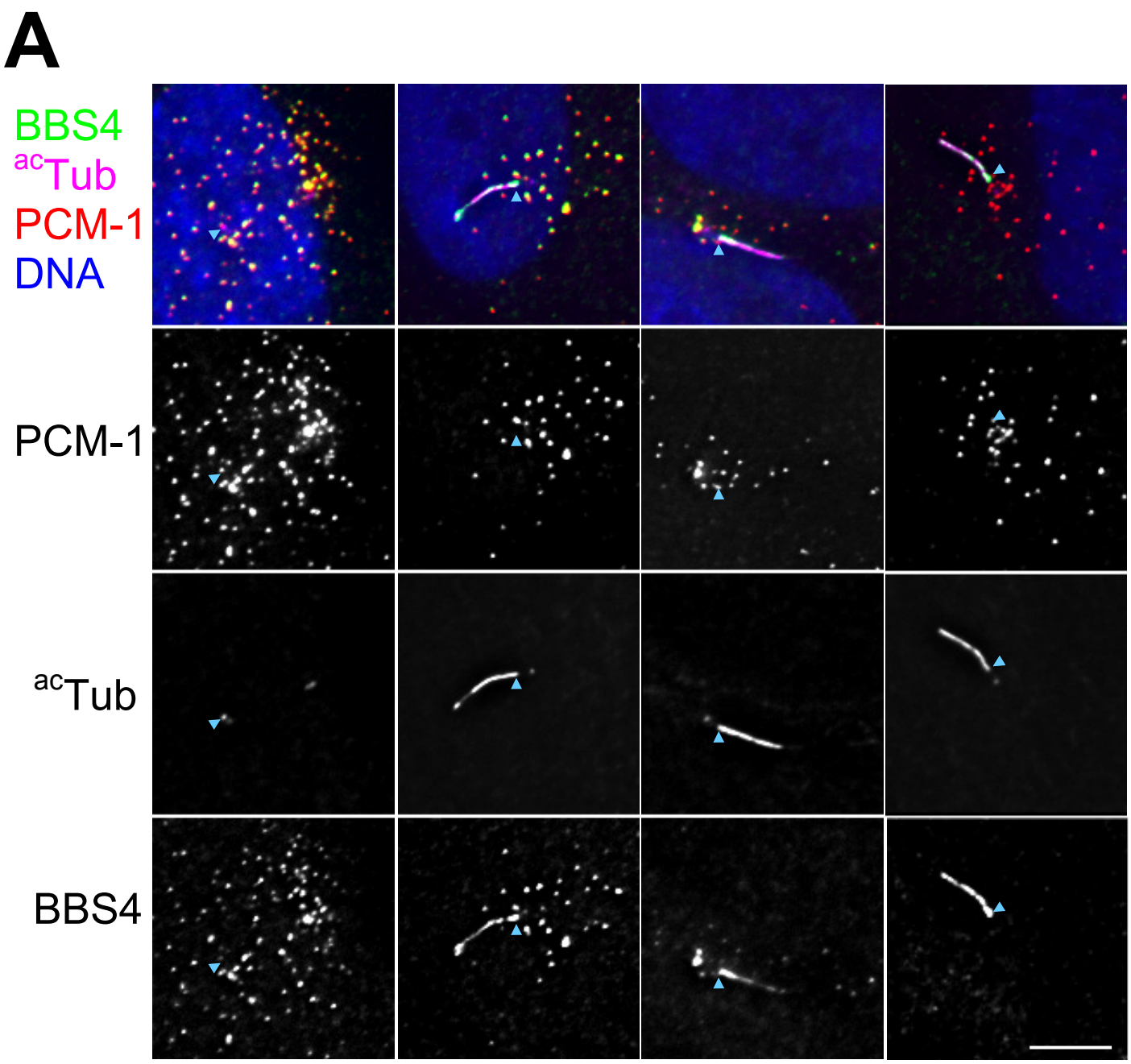

<u>Figure S6</u>: BBS4 is membrane-associated at the cilium but not at centriolar satellites. (A) Gallery of centrosome (leftmost panel) and cilia (three right panels) illustrating the emptying of the centriolar satellite pool of BBS4 upon ciliation. The arrow points to the centrosome or basal body. The presence of a pool of BBS4 spreading beyond the basal body can be appreciated on the three right panels. These images were not deconvolved and correspond to a single focal plane.

B

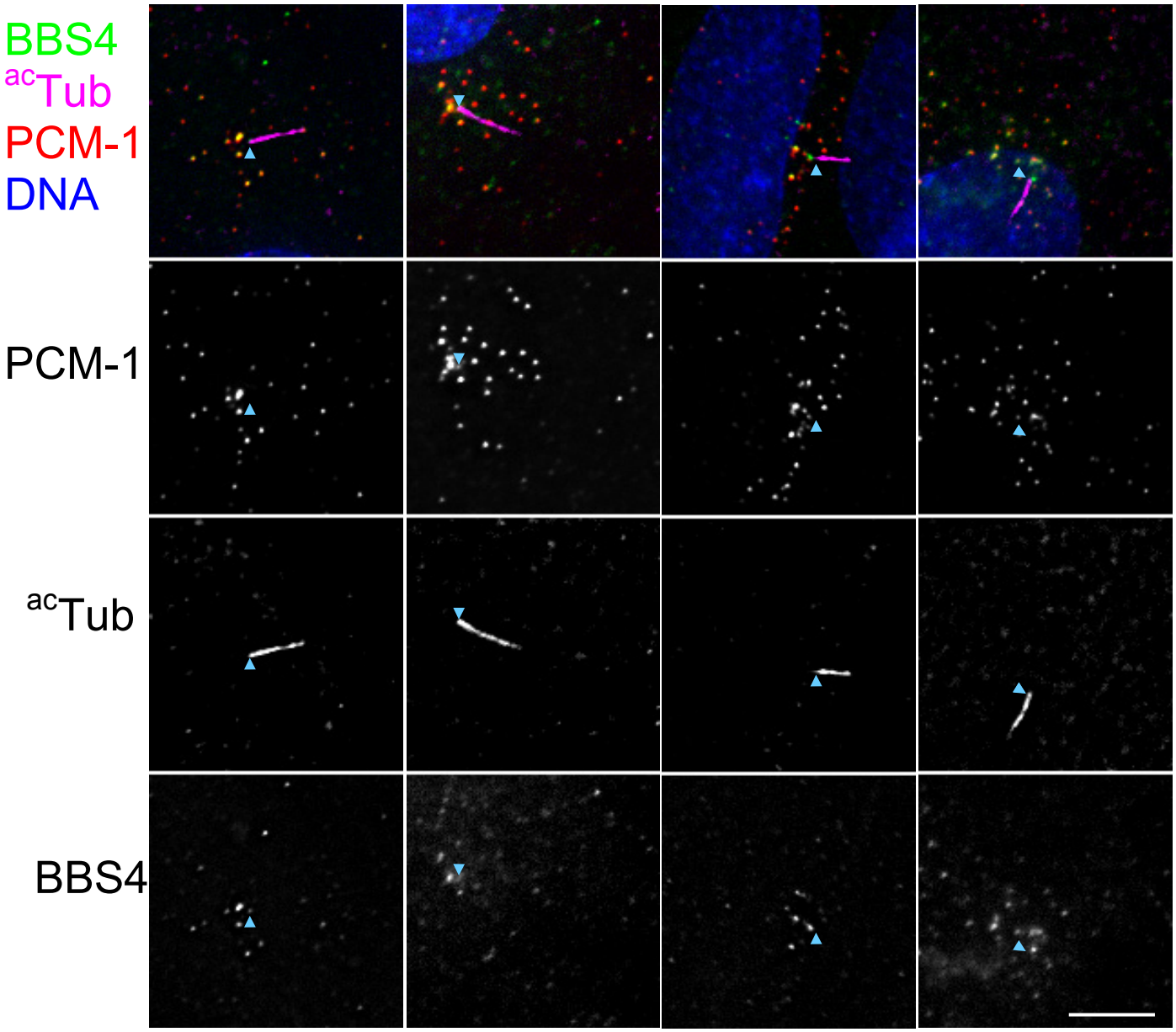

Figure S6 (followed): (B) Gallery of pre-extracted cilia illustrating the membrane association of BBS4 in the cilium. The arrows points to the basal bodies. Scale bar = 5 μm.

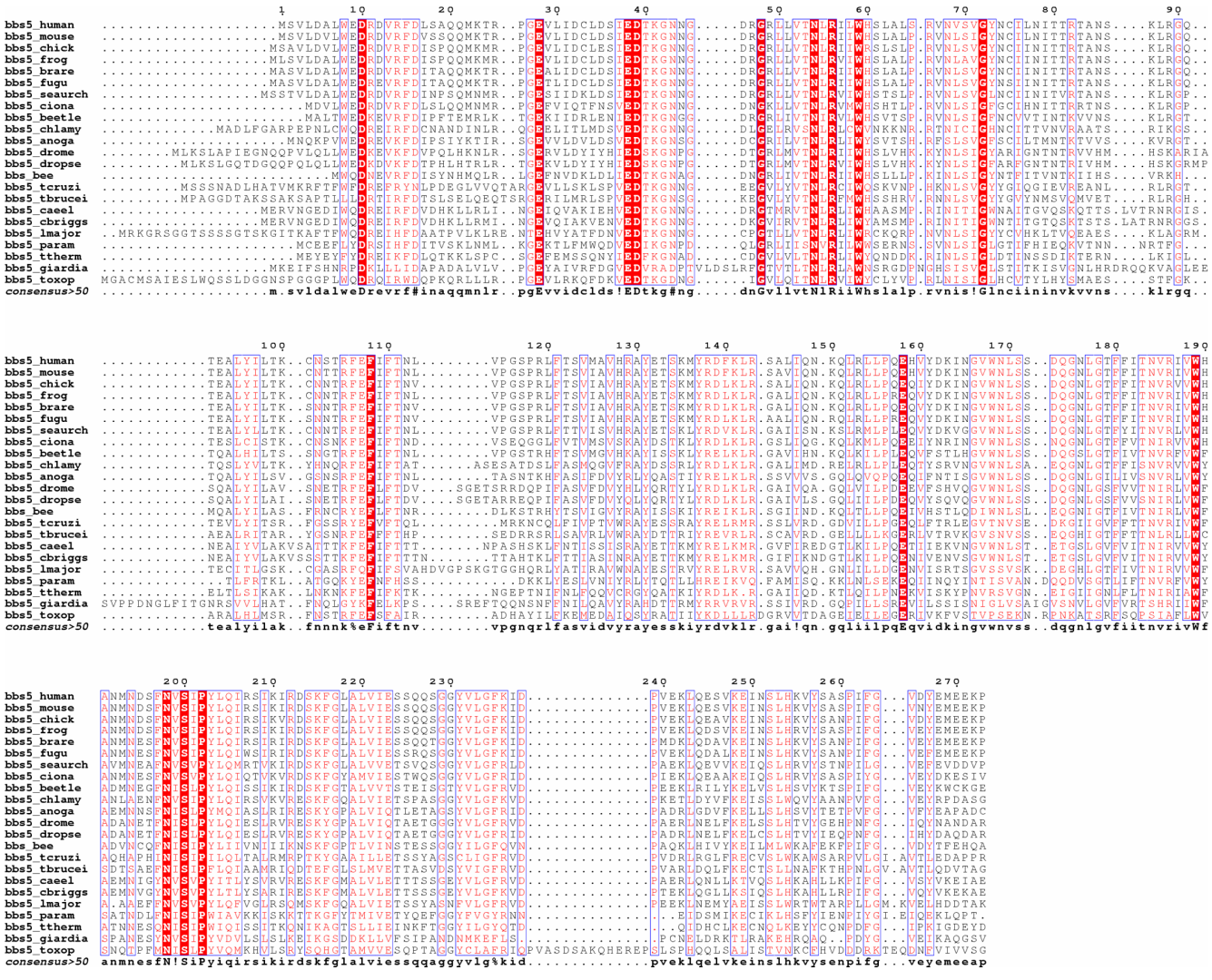

Figure S7: (A) Evolutionarily diverse sequence alignment of twenty-three BBS5 orthologues harvested from sequence databases by iterative PsiBLAST searches. Figure composed with ESPript (Gouet et al., 1999) with sequence conservation coloring by BLOSUM62 comparison matrix. The alignment comprises the double PH-like domains of human BBS5 (amino acids 1-283) described in Fig. 5A.

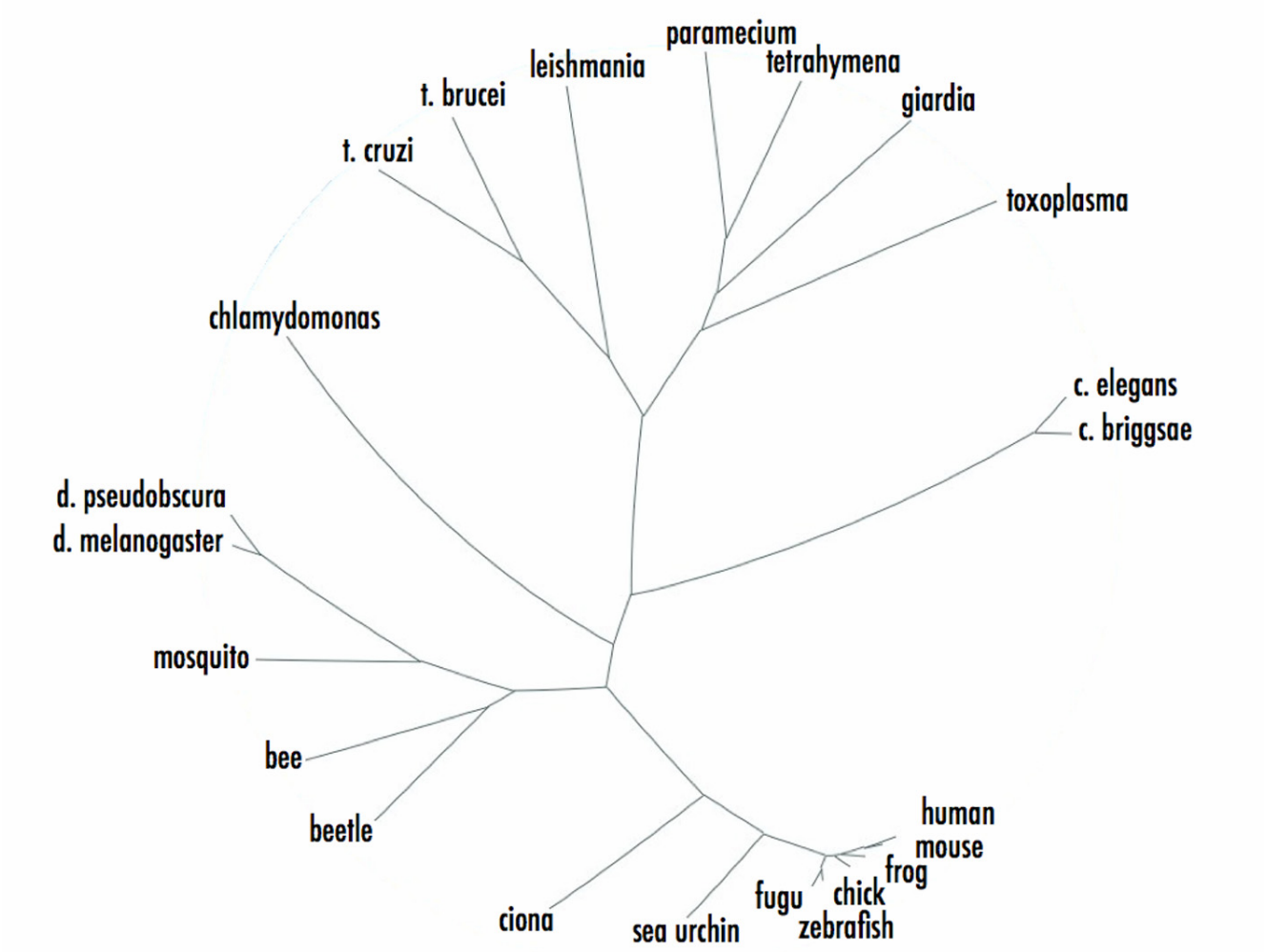

Figure S7 (followed): (B) Phylogenetic tree of BBS5 orthologs derived from the alignment by Neighbor-joining method within ClustalX (Thompson et al., 1997) and displayed using HyperTree (Bingham and Sudarsanam, 2000).

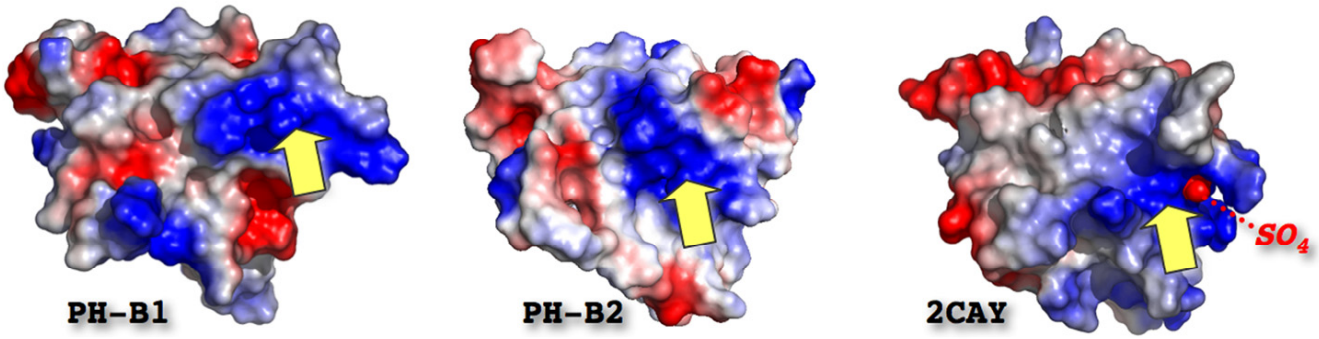

Figure S7 (followed): (C) Likely phosphoinositide-binding pockets of BBS5 PH-B1 and PH-B2 domains are indicated by basic (blue) electrostatic potential surface in an area similar to defined pocket of the GLUE domain (where a bound sulfate ion is labeled).

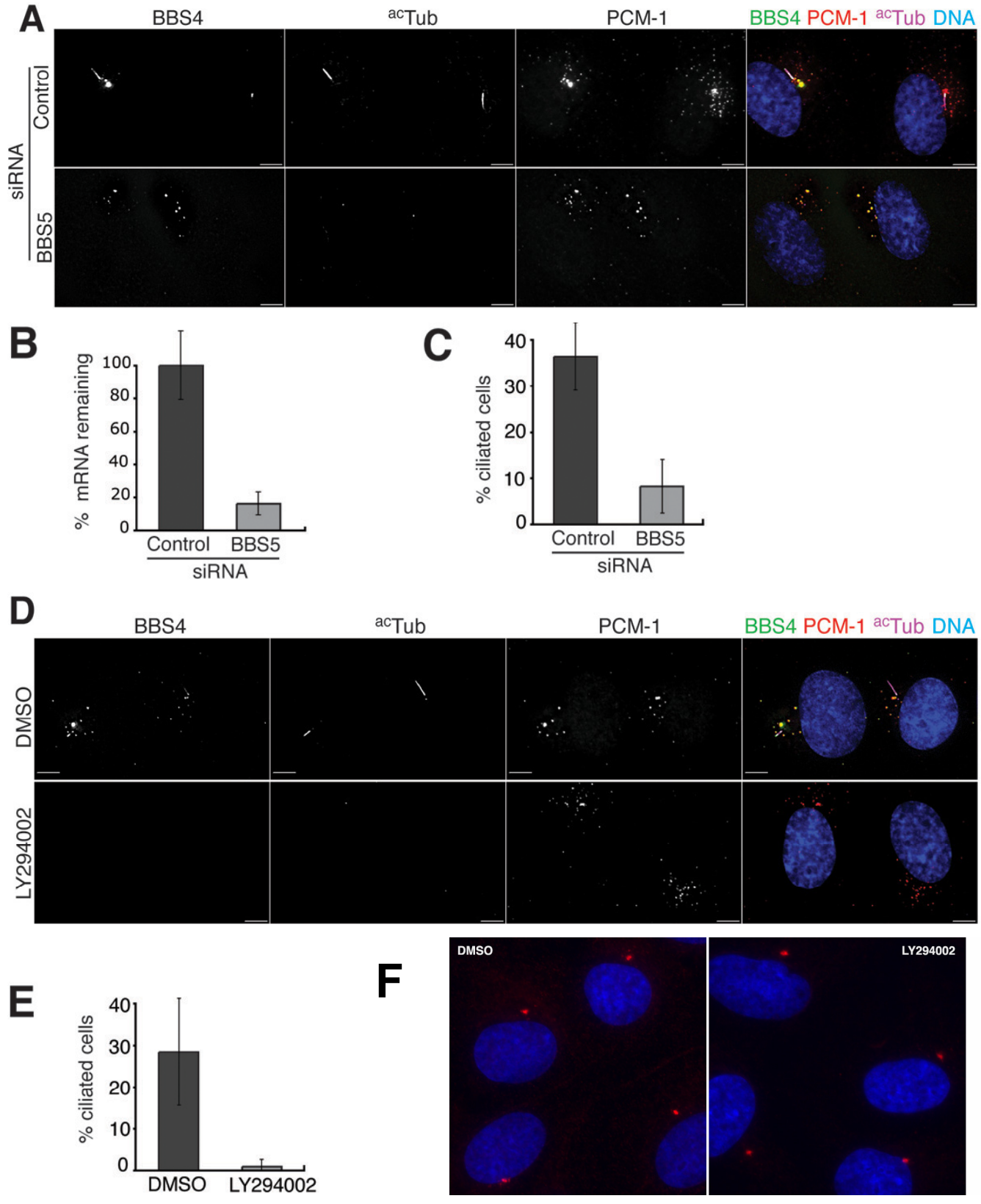

<u>Figure S8</u>: BBS5 and 3-phosphoinositides are necessary for ciliogenesis.
(A) BBS5 is required for ciliogenesis. RPE-[^{LAP}BBS4] cells depleted of BBS5 by siRNA or control depleted cells were allowed to grow a primary cilium and immunostained for GFP (^{LAP}BBS4, green), PCM-1 (red) and acetylated α-tubulin (violet). Nuclei were stained with

Hoechst 33258 (blue). Acetylated α-tubulin is present in the primary cilium (top panel) and at the centrioles (lower panels). Scale bar= 5 μm. BBS5 message abundance was analyzed by qRT-PCR in (B) and cilia were counted in (C). 36.4% (59/161) of control siRNA treated cells were ciliated vs. 8.2% (17/198) of BBS5 siRNA treated cells. (D) Pharmacological inhibition of PI(3)kinase prevents cilium formation. Cells were treated with the PI(3)kinase inhibitor LY294002 or with carrier (DMSO) for 24 h while ciliogenesis was induced by serum deprivation. Cells were immunostained for GFP (green), PCM-1 (red) and acetylated a-tubulin (violet). Nuclei were stained with Hoechst 33258 (blue). Scale bar= 5 μm. Cilia were counted in (E). 28.4% (102/356) of DMSO treated cells were ciliated vs. 0.9% (2/235) of LY294002 treated cells. (F) LY294002 treatment does not affect pericentrin localization. Cells were immunostained for pericentrin (red) and nuclei were stained with Hoechst 33258 (blue).

A

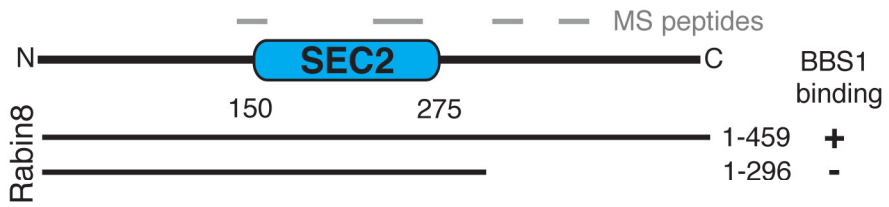

B

gi|10438974 **MS/MS Spectra:** 2 **Sum TIC:** 1.6e4 **Avg TIC:** 7.9e3 **Cov:** 5.0% **Uniq:** 2
unnamed protein product [Homo sapiens]

Sequence	Reference	TIC	Sf	D	Scan
(K) IDVLQAEVAALK	gi|10438974 +22	5.7e3	0.81	b	5455
(K) EADLSLYNEFR	gi|10438974 +15	10.0e3	0.04	b	5045

gi|10438974 **MS/MS Spectra:** 4 **Sum TIC:** 8.1e4 **Avg TIC:** 2.0e4 **Cov:** 11.8% **Uniq:** 4
unnamed protein product [Homo sapiens]

Sequence	Reference	TIC	Sf	Scan
(K) IDVLQAEVAALK	gi|10438974 +20	1.9e4	0.87	4700
(K) IYQEDIFPCLTFSK	gi|10438974 +10	1.9e4	0.84	5120
(K) TLVLSSSPTSPTQEPLPGGK	gi|10438974 +13	1.4e4	0.82	3888
(R) SPSVLEVR	gi|10438974 +14	2.9e4	0.76	3213

C

>gi|28274699| Rabin8/Rab3IP alpha1 [Homo sapiens]

MANDPLEGFHEVNLASPTSPDLLGVYESGTQEQTTSPSVIYRPHPSALSSVPIQANALDVSELPTQPVYSS
PRRLNCAEISSISFHVTDPAPCSTSGVTAGLTKLTTRKDNYNAEREFLQGATITEACDGSDDIFGLSTDSL
SRLRSPSV**LEVREKGYERLKEELAKAQRELKLKDEECERLSKVRDQLGQELEELTASLFEEAHKMVREANI
KQATAEKQLKEAQGKIDVLQAEVAALKTLVLSSSPTSPTQEPLPGGKTPFKKGHTRNKSTSS**AMSGSHQDL
SVIQPIVKDCKEADLSLYNEFRLWKDEPTMDRTCPFLDKIYQEDIFPCLTFSKSELASAVLEAVENNTLSI
EPVGLQPIRFVKASAVECGGPKKCALTGQSKSCKHRIKLGDSSNYYYISPFCRYRITSVCNFFTYIRYIQQ
GLVKQQDVDQMFWEVMQLRKEMSLAKLGYFKEEL

D

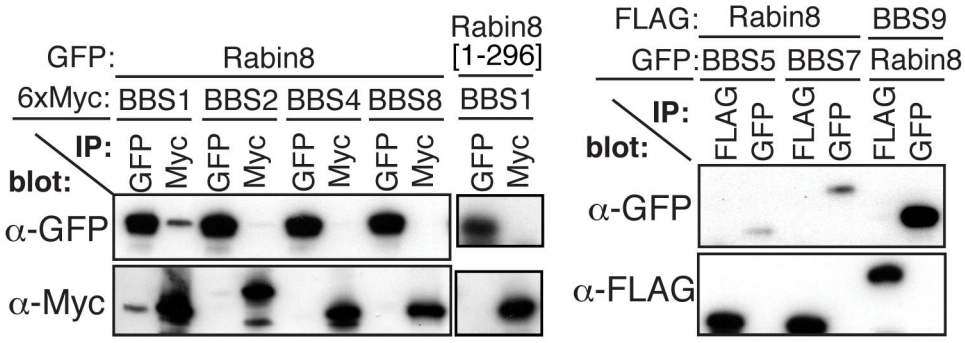

Figure S9: Rabin8 interacts with the BBSome.

(A) Schematic organization of Rabin8. The position of the peptides identified by LC-MS/MS of BBSome preparation is indicated on top. A summary of the domain mapping studies is indicated below. (B) Raw data from LC-MS/MS analysis of BBS4-associated proteins. For the upper panel, a band corresponding to a molecular weight range between 54 and 58 kDa was excised. For the lower panel, the entire eluate was analyzed as one sample. gi|10438974 corresponds to a Genebank entry identical to Rabin8/Rab3IP isoform α1 (C) The position of the peptides identified by LC-MS/MS is underlined and the Sec2 domain is highlighted in **BOLD**. (D) Rabin8 specifically interacts with BBS1. GFP-, FLAG-, and Myc-tagged BBSome subunits were co-transfected with GFP- and FLAG-tagged Rabin8-α1 into 293T cells and reciprocal immunoprecipitations were conducted to detect protein-protein interactions. While Rabin8-α1 binds to BBS1, Rabin8-α1[1-296] fails to interact with BBS1.

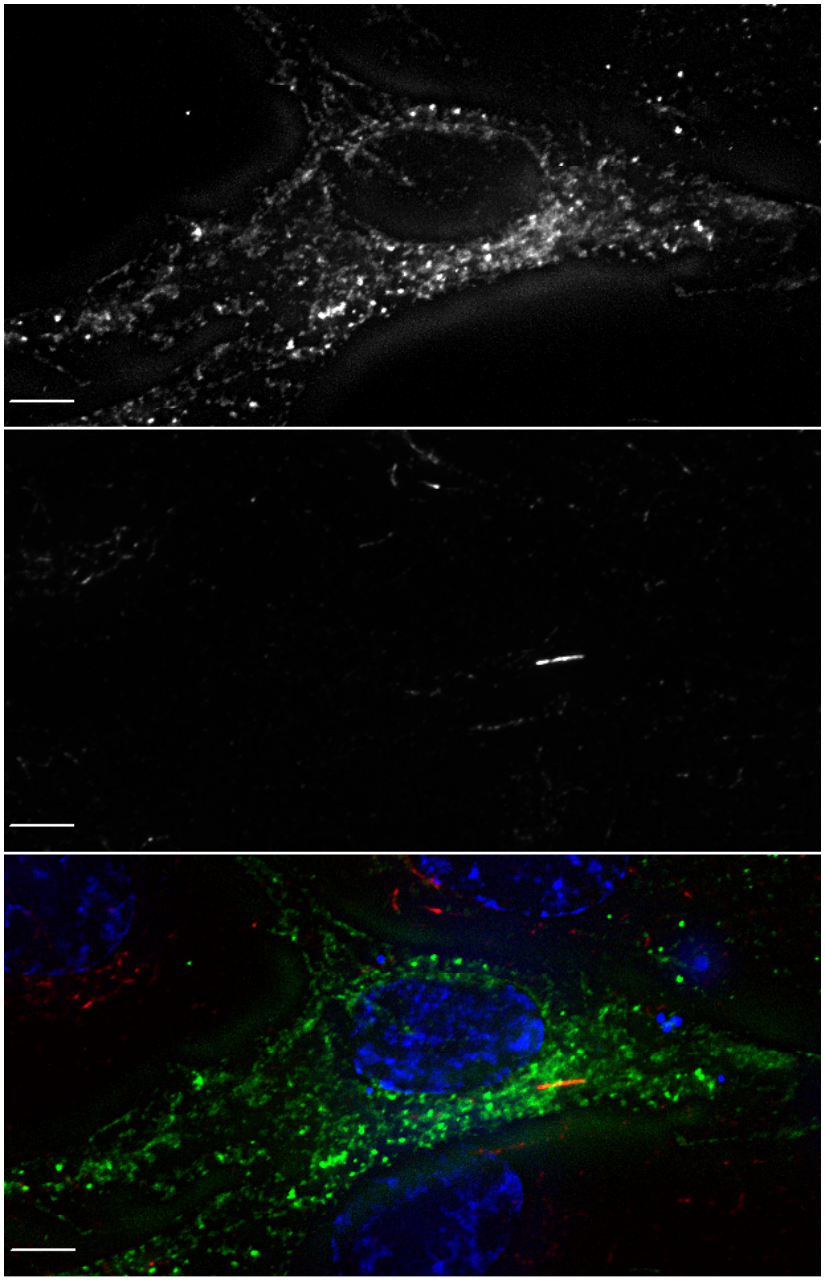

<u>Figure S10</u>: Rab8[T22N] does not enter the primary cilium.
One of the rare cells that grew a cilium despite expressing GFP-Rab8[T22N] is shown. 48h after transfection, cells were immunostained for GFP, PCM-1 and acetylated α-tubulin. Nuclei were stained with Hoechst 33258. Scale bar= 5 μm.

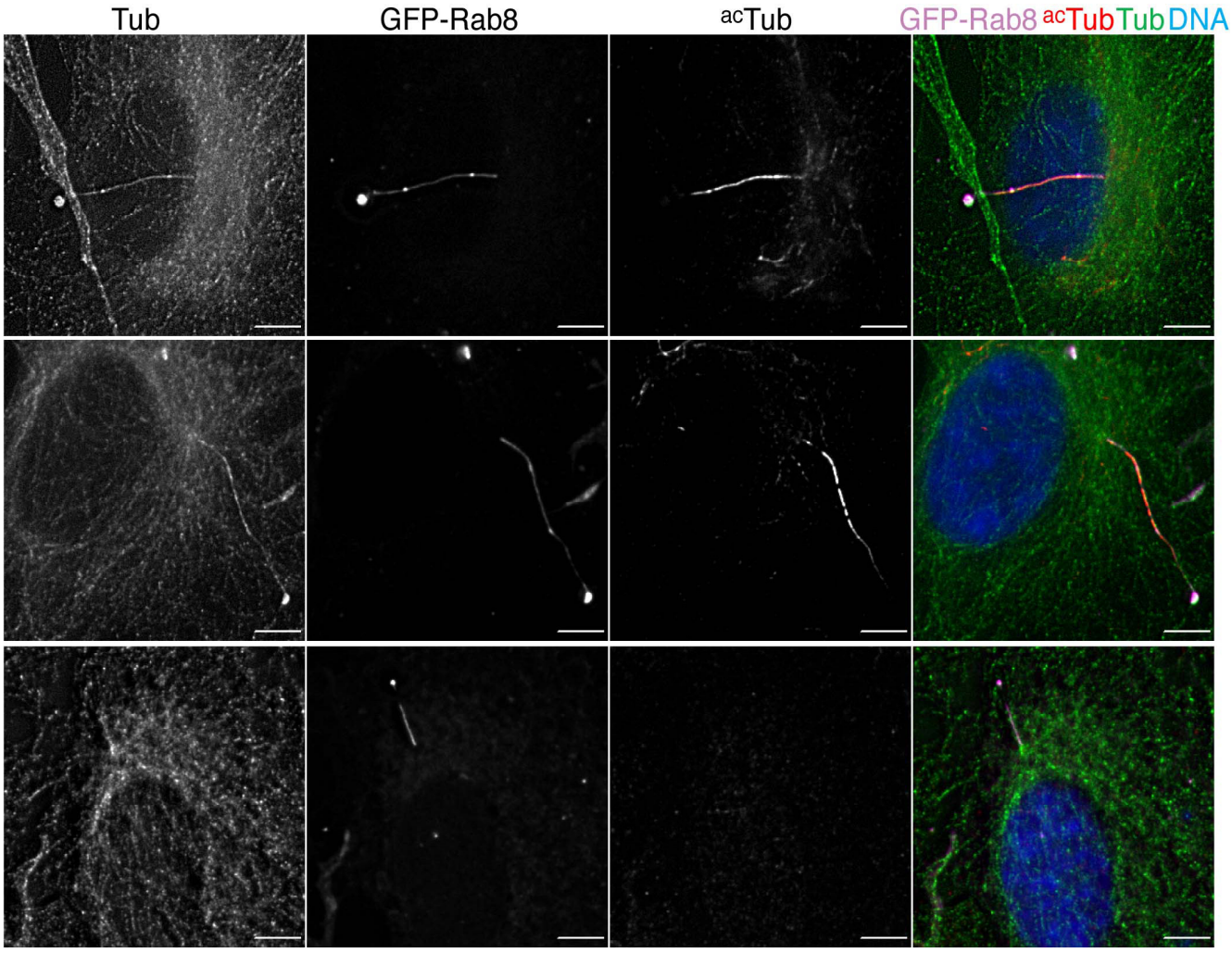

<u>Figure S11</u>: Rab8-positive cilium extensions are positive for α-tubulin despite being negative for acetylated α-tubulin.

pEGFP-Rab8 transfected-cells were immunostained for GFP, α-tubulin and acetylated α-tubulin. Nuclei were stained with Hoechst 33258. Scale bar= 5 μm.

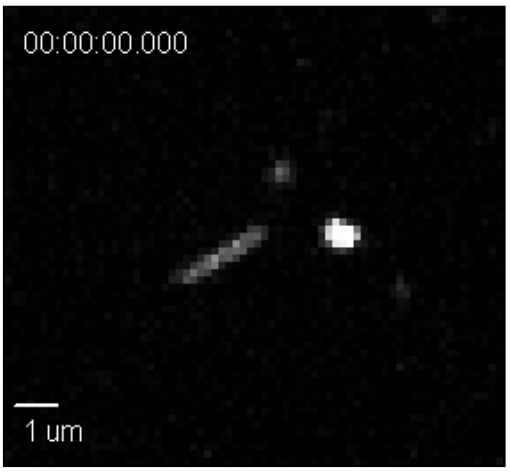
00:00:00.000
1 um

Supplemental Methods

Fold recognition and structural modeling of BBS5

BBS5 orthologue sequences were harvested by iterative PsiBLAST runs (Altschul et al., 1997), and the resulting alignment was used to drive sensitive repeat detection by the HHrep program (Soding et al., 2006) and secondary structure prediction by PsiPRED (McGuffin et al., 2000). The Genesilico fold recognition metaserver (Kurowski and Bujnicki, 2003) and HHpred (Soding et al., 2005) confirmed the fold relationship of the BBS5 BOO modules with the MTMR2 PH-GRAM and Vps36 GLUE PH-like domains. Comparative models of each BOO domain were built with MODELLER (Sali and Blundell, 1993) using the superposition of the latter two template structures (PDB ID 1ZSQ and 2CAY, respectively) by the SSM program (Krissinel and Henrick, 2004). Structures were manipulated and visualized with Pymol (DeLano Scientific).

Co-immunoprecipitation assays.

Plasmids encoding BBSome subunits tagged with HA, Myc or FLAG were co-transfected into HEK293T cells. Cells were lyzed 48 h post-transfection in PBS + 1% Triton-X100 with Complete® protease inhibitors (Roche) and lysates were spun at 14,000 rpm for 15 min at 4ºC. The supernatants were incubated with Protein-G-Sepharose beads to reduce non-specific background. Cleared and pre-adsorbed lysates were incubated with an antibody against a given tag (HA, My, FLAG) for 4 h at 4ºC, mixed with Protein-G-Sepharose beads for another 4 hrs and beads were washed three times with lysis buffer before elution in SDS sample buffer. Tagged proteins were detected by western blotting.

Live cell imaging.

RPE-[LAP-BBS4] cells were grown on glass-bottom Labtek chambers and serum starved to induce ciliation. Cells with a horizontal cilium were imaged with a spinning-disk confocal microscope with 200 ms exposures and 0.9 s intervals.

References for supplemental data:

Altschul, S. F., Madden, T. L., Schaffer, A. A., Zhang, J., Zhang, Z., Miller, W., and Lipman, D. J. (1997). Gapped BLAST and PSI-BLAST: a new generation of protein database search programs. Nucleic Acids Res *25*, 3389-3402.

Ansley, S. J., Badano, J. L., Blacque, O. E., Hill, J., Hoskins, B. E., Leitch, C. C., Kim, J. C., Ross, A. J., Eichers, E. R., Teslovich, T. M*., et al.* (2003). Basal body dysfunction is a likely cause of pleiotropic Bardet-Biedl syndrome. Nature *425*, 628-633.

Badano, J. L., Leitch, C. C., Ansley, S. J., May-Simera, H., Lawson, S., Lewis, R. A., Beales, P. L., Dietz, H. C., Fisher, S., and Katsanis, N. (2006). Dissection of epistasis in oligogenic Bardet-Biedl syndrome. Nature *439*, 326-330.

Bingham, J., and Sudarsanam, S. (2000). Visualizing large hierarchical clusters in hyperbolic space. Bioinformatics *16*, 660-661.

Gouet, P., Courcelle, E., Stuart, D. I., and Metoz, F. (1999). ESPript: analysis of multiple sequence alignments in PostScript. Bioinformatics *15*, 305-308.

Kim, J. C., Badano, J. L., Sibold, S., Esmail, M. A., Hill, J., Hoskins, B. E., Leitch, C. C., Venner, K., Ansley, S. J., Ross, A. J*., et al.* (2004). The Bardet-Biedl protein BBS4 targets cargo to the pericentriolar region and is required for microtubule anchoring and cell cycle progression. Nat Genet *36*, 462-470.

Krissinel, E., and Henrick, K. (2004). Secondary-structure matching (SSM), a new tool for fast protein structure alignment in three dimensions. Acta Crystallogr D Biol Crystallogr *60*, 2256-2268.

Kurowski, M. A., and Bujnicki, J. M. (2003). GeneSilico protein structure prediction meta-server. Nucleic Acids Res *31*, 3305-3307.

McGuffin, L. J., Bryson, K., and Jones, D. T. (2000). The PSIPRED protein structure prediction server. Bioinformatics *16*, 404-405.

Sali, A., and Blundell, T. L. (1993). Comparative protein modelling by satisfaction of spatial restraints. J Mol Biol *234*, 779-815.

Siegel, L. M., and Monty, K. J. (1966). Determination of molecular weights and frictional ratios of proteins in impure systems by use of gel filtration and density gradient centrifugation. Application to crude preparations of sulfite and hydroxylamine reductases. Biochim Biophys Acta *112*, 346-362.

Soding, J., Biegert, A., and Lupas, A. N. (2005). The HHpred interactive server for protein homology detection and structure prediction. Nucleic Acids Res *33*, W244-248.

Soding, J., Remmert, M., and Biegert, A. (2006). HHrep: de novo protein repeat detection and the origin of TIM barrels. Nucleic Acids Res *34*, W137-142.

Thompson, J. D., Gibson, T. J., Plewniak, F., Jeanmougin, F., and Higgins, D. G. (1997). The CLUSTAL_X windows interface: flexible strategies for multiple sequence alignment aided by quality analysis tools. Nucleic Acids Res *25*, 4876-4882.